



HAL
open science

Platelets Facilitate the Wound-Healing Capability of Mesenchymal Stem Cells by Mitochondrial Transfer and Metabolic Reprogramming

Jennyfer Levoux, Alexandre Prola, Peggy Lafuste, Marianne Gervais, Nathalie Chevallier, Zeynab Koumaiha, Kaouthar Kefi, Laura Braud, Alain Schmitt, Azzedine Yacia, et al.

► To cite this version:

Jennyfer Levoux, Alexandre Prola, Peggy Lafuste, Marianne Gervais, Nathalie Chevallier, et al.. Platelets Facilitate the Wound-Healing Capability of Mesenchymal Stem Cells by Mitochondrial Transfer and Metabolic Reprogramming. *Cell Metabolism*, 2021, 33 (2), pp.283-299.e9. 10.1016/j.cmet.2020.12.006 . hal-03876917

HAL Id: hal-03876917

<https://hal.science/hal-03876917v1>

Submitted on 13 Feb 2023

HAL is a multi-disciplinary open access archive for the deposit and dissemination of scientific research documents, whether they are published or not. The documents may come from teaching and research institutions in France or abroad, or from public or private research centers.

L'archive ouverte pluridisciplinaire **HAL**, est destinée au dépôt et à la diffusion de documents scientifiques de niveau recherche, publiés ou non, émanant des établissements d'enseignement et de recherche français ou étrangers, des laboratoires publics ou privés.



Distributed under a Creative Commons Attribution - NonCommercial 4.0 International License

Platelets facilitate the wound healing capability of mesenchymal stem cells by mitochondrial transfer and metabolic reprogramming

Jennyfer Levoux^{1,#}, Alexandre Prola^{1,2,#}, Peggy Lafuste^{1,#}, Marianne Gervais¹, Nathalie Chevallier^{1,3}, Zeynab Koumaiha¹, Kaouthar Kefi¹, Laura Braud¹, Alain Schmitt⁴, Azzedine Yacia⁴, Aurélie Schirmann¹, Barbara Hersant^{1,5}, Mounia Sid-Ahmed^{1,5}, Sabrina Ben Larbi⁶, Katerina Komrskova^{7,8}, Jakub Rohlena⁷, Frederic Relaix^{1,2}, Jiri Neuzil^{7,10} and Anne-Marie Rodriguez^{1,§,*}

¹Univ Paris Est Creteil, INSERM, IMRB, F-94010 Créteil, France; ²EnvA, IMRB, F-94700 Maisons-Alfort, France ; ³Etablissement Français du Sang, 94017, Créteil, France; ⁴Université de Paris, Institut Cochin, INSERM, CNRS, F-75014 PARIS, France; ⁵AP-HP, Hôpital Henri Mondor-A. Chenevier, Service de chirurgie plastique et maxillo-faciale, Créteil, France; ⁶Institut NeuroMyoGène, Université Claude Bernard Lyon 1, Univ Lyon, CNRS UMR 5310, INSERM U1217, Lyon, France; ⁷Institute of Biotechnology, Czech Academy of Sciences, 252 50 Prague-West, Czech Republic; ⁸Department of Zoology, Faculty of Science, Charles University, 128 44 Prague 2, Czech Republic; ⁹APHP, Hôpitaux Universitaires Henri Mondor & Centre de Référence des Maladies Neuromusculaires GNMH, 94000, Créteil, France; ¹⁰School of Medical Science, Griffith University, Southport, Qld 4222, Australia

#These authors contributed equally to this work.

§Lead Contact

*Correspondence: anne-marie.rodriquez@inserm.fr

SUMMARY

Platelets are known to enhance the wound-healing activity of mesenchymal stem cells (MSCs). However, the mechanism by which platelets improve the therapeutic potential of MSCs has not been elucidated. Here, we provide evidence that, upon their activation, platelets transfer respiratory-competent mitochondria to MSCs primarily via dynamin-dependent clathrin-mediated endocytosis. We found that this process enhances the therapeutic efficacy of MSCs following their engraftment in several mouse models of tissue injury including full-thickness cutaneous wound and dystrophic skeletal muscle. By combining *in vitro* and *in vivo* experiments, we demonstrate that platelet-derived mitochondria promote the pro-angiogenic activity of MSCs via their metabolic remodeling. Notably, we show that activation of the *de novo* fatty acid synthesis pathway is required for increased secretion of pro-angiogenic factors by platelet-preconditioned MSCs. These results reveal a new mechanism by which platelets potentiate MSC properties and underline the importance of testing platelet mitochondria quality prior to their clinical use.

INTRODUCTION

The use of mesenchymal stem cells (MSCs) holds great promise for the repair of tissue damage such as hard-to-heal wounds that represent a major public health burden (Lindholm and Searle, 2016). MSCs can be easily isolated in clinically required purity from several tissues, including bone marrow and adipose tissue (Yong et al., 2018), and they can be expanded on a large scale *in vitro* owing to their strong proliferative potential (D'Ippolito et al., 2004; Rodriguez et al., 2005). In addition, MSCs possess regenerative properties, a prominent one being their ability to promote re-vascularization of injured tissue by means of secreting pro-angiogenic soluble factors (Figeac et al., 2014; Shi et al., 2019; Yong et al., 2018). Beneficial effects of MSC engraftment have been reported for a number of animal disease models (Chen et al., 2003; Gandia et al., 2008; Rehman et al., 2004). However, the positive results obtained in animal studies are not consistently reproduced in clinical trials, indicating the need to improve the efficacy of MSC-based therapies to achieve significant functional recovery of damaged tissues (Golchin et al., 2019; Rowart et al., 2015; Yong et al., 2018). With this in mind, several groups have been exploring whether platelets, platelet-containing preparations such as platelet-rich plasma (PRP) or platelet lysates can be used to promote the regenerative potential of MSCs (Andia et al., 2018; Chevallier et al., 2010; Henschler et al., 2019; Leotot et al., 2013; Tobita et al., 2015).

Platelets are blood-circulating components derived from megakaryocytes present in bone marrow that play a major role in several (patho)physiological processes such as thrombosis, hemostasis, inflammation and wound healing (Holinstat, 2017). These anucleated cells contain secretory organelles including alpha granules containing various proteins and growth factors. Platelets also comprise functional mitochondria that provide energy for their metabolism (Gremmel et al., 2016). Several studies have reported that PRP can be used as an adjuvant to improve the therapeutic efficacy of MSCs (Hersant et al., 2019; Mahmoudian-Sani et al., 2018; Qian et al., 2017). We have shown that PRP stimulates proliferation and pro-angiogenic properties of MSCs and improves their survival following exposure to oxidative stress (Hersant et al., 2019). The 'healing' effects exerted by platelets on MSCs are attributed to the release of growth factors (Chicharro-Alcántara et al., 2018; Marx, 2004). However, their exact contribution to MSCs activation is unclear.

Mitochondria play a critical role in the regulation of metabolic processes that govern the function and fate decision of stem cells of adult, embryonic/pluripotent or cancer origin (Bahat and Gross, 2019; Peiris-Pagès et al., 2016; Porporato et al., 2018; Wanet et al., 2015). An important function of mitochondria is to generate metabolites from the tricarboxylic acid

(TCA) cycle that are essential for anabolic processes. For instance, citrate that is produced in the TCA cycle by citrate synthase from acetyl-CoA and oxaloacetate is an important precursor for fatty acid synthesis. This requires several cytosolic enzymes including ATP citrate lyase (ACLY) converting citrate into acetyl-coenzyme A (acetyl-CoA), acetyl-CoA carboxylase (ACC) converting acetyl-CoA into malonyl-CoA, and fatty acid synthase (FAS) forming fatty acids from malonyl-CoA (Spinelli and Haigis, 2018). The importance of *de novo* fatty acid synthesis in proliferation and angiogenesis has been documented for cancer stem cells (Röhrig and Schulze, 2016) and endothelial cells (Bruning et al., 2018), as well as for pluripotency in embryonic stem cells or induced-pluripotent stem cells (Wang et al., 2017). However, the impact of *de novo* fatty acid synthesis on the behavior and function of MSCs have not been studied.

In addition to their intracellular metabolic functions, mitochondria can also affect the functions of neighboring cells. These effects are supported by the capacity of mitochondria to translocate from one cell to the other, as recently demonstrated both *in vitro* and *in vivo* (Nakhle et al., 2020; Rodriguez et al., 2018). In particular, the acquisition of MSC mitochondria by damaged cells, such as cardiac or lung epithelial cells, has been reported to rescue these cells by improving their respiratory function and energy metabolism (Acquistapace et al., 2011; Ahmad et al., 2014; Islam et al., 2012; Mahrouf-Yorgov et al., 2017) while mitochondria transfer from damaged cells to MSCs has been shown to stimulate the cytoprotective function of the latter (Mahrouf-Yorgov et al., 2017). Here, we explored whether platelet mitochondria can be transferred to MSCs following their exposure to platelets and their role in activation of the MSC's regenerative properties. Our results indicate that mitochondria released by platelets following their activation stimulate pro-angiogenic properties of MSCs via metabolic remodeling including enhanced *de novo* fatty acid synthesis.

RESULTS

Mitochondria released by platelets stimulate wound-healing efficacy of MSCs.

To determine whether mitochondria transfer from platelets to MSCs, we co-cultured MSCs for 24 h with labelled human platelets with Mitotracker Green or isolated mitochondria tagged with red fluorescence protein from C57BL/6J^{su9-DsRed2} mice. We next evaluated the presence of human or mouse platelet-derived mitochondria in MSCs using confocal microscopy and flow cytometry (Figure 1A and B). In addition, we found that the mitotracker

fluorescent signal indicating the level of mitochondria derived from human platelets and transferred to MSCs was dependent on the number of platelets in the co-culture experiment (Figure 1C). Previous reports document that platelets can release mitochondria to membrane-encapsulated microparticles of more than 500 nm in size or as free organelles (Boudreau et al., 2014; Marcoux et al., 2017). We therefore analyzed the transfer of human platelet mitochondria labelled with Mitotracker Green to human MSCs using transwells (TW) with 0.4 μm pore-size inserts separating MSCs from activated platelets. Under this experimental setting, transfer of mitochondria from human platelets to MSCs was partially inhibited (Figure 1D and E), suggesting that MSCs internalized these organelles in their free form or contained in microvesicles. Consistent with these observations, transmission electron microscopy (TEM) analysis revealed that platelets, whose morphology is typical for a reversible aggregation state, released ‘mitochondria-like’ double membrane structures with the size ranging from 0.2 to more than 1 μm and that these structures were internalized by MSCs (Supplementary Figure 1A and B).

We next investigated whether mitochondria transferred from platelets to MSCs modulate their wound-healing activity. We grafted human MSCs into mouse wounds, in combination with untreated human platelets or with human platelets previously treated with rotenone and antimycin A (ROT/AA) to inhibit their mitochondrial respiration. The rate of wound closure determined by macroscopic analysis on days 3 and 7 after the injury was significantly higher in animals treated with human MSCs and human platelets compared to the cohorts of animals that received either saline solution, platelets alone or MSCs alone (Figure 1F and G), confirming that platelets improved the therapeutic efficacy of MSCs. In contrast, human platelets treated with ROT/AA failed to stimulate the wound-healing activity of MSCs (Figure 1F and G).

Platelet-derived mitochondria are transferred to MSCs via dynamin-dependent clathrin-mediated endocytosis and activate mitochondrial fusion in recipient MSCs.

We tested whether the impaired ability of ROT/AA-treated platelets to stimulate the wound-healing activity of MSCs is due to possible dysfunctional transfer of mitochondria from platelets to MSCs. TEM analysis showed that, similarly to intact platelets, ROT/AA-treated platelets exhibited both “activated” morphology and comprised mitochondria with cristae (Supplementary Figure 1A), and that they released mitochondria in free as well encapsulated forms (Supplementary Figure 1B and C). In addition, as documented in Figure 1A, D and E, the number of platelet-derived mitochondria taken up by MSCs was similar for either human

untreated or ROT/AA-treated platelets that were labeled with Mitotracker Green or for murine platelets isolated from C57BL/6J^{su9-DsRed2} mice. We then investigated the process by which MSCs internalized platelet mitochondria and found that their transfer to MSCs was almost completely suppressed by dynasore, an inhibitor of dynamin-dependent clathrin-mediated endocytosis that does not affect the viability of MSCs (Supplementary Figure 1D and E). We also observed a minor contribution of macropinocytosis and caveolae-mediated endocytosis in internalization of platelet mitochondria by MSCs, following treatment with either the macropinocytosis inhibitor 5-[N-ethyl-N-isopropyl]-amiloride (EIPA) or blockers of caveolae-mediated endocytosis including B-cyclodextrin, genistein and nystatin (Supplementary Figure 1F). In contrast to a previous study showing that mitochondria transfer from engrafted MSCs to epithelial lung cells requires attachment of MSCs to the alveolar epithelium through connexin 43 gap junctions (Islam et al., 2012), we observed no effect of the connexin 43 mimetic peptide Gap26 (Supplementary Figure 1F). In addition, mitochondria from ROT/AA-treated platelets were shown to be internalized by MSCs in a similar fashion to those from intact platelets (Supplementary Figure D and data not shown).

Finally, we investigated the morphology of the mitochondrial network of MSCs after endocytosis of platelet mitochondria. TEM analysis revealed that untreated MSCs had low number of small mitochondria, while MSCs exposed to intact or ROT/AA-treated platelets exhibited numerous and hyperfused mitochondria detectable as soon as 2 hours after the co-culture (Supplementary Figure 1G). This was accompanied by increased expression of mitofusin-2 in MSCs co-cultured with intact or ROT/AA-treated platelets (Supplementary Figure 1H). Overall, these data indicate that the failure of ROT/AA-treated platelets to stimulate repair function of MSCs cannot be explained by reduced efficacy of their transfer or internalization by MSCs or by differences in promoting mitochondrial fusion activation in MSCs.

Platelet-derived mitochondria do not stimulate differentiation or the immune-regulatory function of MSCs.

As MSCs are known to differentiate *in vitro* into adipocytes and osteoblasts (Rodriguez et al., 2005), we investigated whether the plasticity potential of engrafted MSCs was affected by intact or ROT/AA-treated platelets. However, no transcriptional expression of human adipocyte (adipocyte-type fatty acid-binding protein and peroxisome proliferator-activated receptor gamma 2) and osteoblast (osteocalcin (OC) and osteopontin (OP)) markers was detected in mouse wounds on days 3 and 7 post-grafting, indicating that MSCs differentiated

neither into adipocytes nor into osteoblasts in mouse wounds when they were grafted alone or co-grafted with intact or ROT/AA-treated platelets.

To exclude the possibility of ectopic bone formation from mouse cells in wounds treated with human MSCs, human platelets or both, we examined transcription of mouse OC and OP genes and found their expression was not elevated in wounds treated with MSCs, platelets or both compared to saline-treated wounds (Supplementary Figure 2A and B). We also performed longer follow-up experiments with MSCs and platelets subcutaneously injected with or without bone scaffold in severe combined immunodeficient (SCID) mice. We found that after 7 weeks, bone formation occurred only in the presence of the biomaterial (Supplementary Figure 2C and D) supporting the conclusion that treatments with human MSCs, human platelets or both do not promote bone formation in mouse wounds.

Besides their plasticity, human MSCs also feature immunoregulatory properties counteracting immune rejection in xenogenic hosts, and favoring tissue regeneration (Lee and Song, 2018; Rodriguez et al., 2005). We therefore investigated whether intact or ROT/AA-treated human platelets affect inflammation processes in mouse wounds following engraftment of human MSCs. We found that transcriptional expression of mouse markers for T-lymphocytes (CD8 and CD4), and macrophages (lymphocyte antigen 6C (Ly6C), CD206 and arginase 1 (mArg1)) as well as pro-inflammatory cytokines (IL-1 α , IL-6 and TNF- α) was unchanged (Supplementary Figure 2E), suggesting that combined application of human MSCs with human platelets does not improve wound healing by altering inflammatory processes at the wound site.

Platelet-derived mitochondria are not involved in the proliferative and cytoprotective effects of platelets on MSCs.

To assess whether mitochondria derived from platelets play a role in activating the proliferative potential of MSCs, we evaluated carboxyfluorescein diacetate succinimidyl ester (CFSE) fluorescence of human MSCs 24 h after their exposure to different numbers of human untreated or ROT/AA-treated platelets. We observed a similar decrease of CFSE fluorescence in MSCs under both conditions (Figure 2A). Consistent with these results, expression of the proliferation marker Ki67 mRNA increased in MSCs following their exposure to platelets in a dose-dependent fashion and independent of ROT/AA pre-treatment of platelets, presence of 0.4 μ m pore size TW insert or exposure to dynasore (Figure 2B, C and D). Similar increase of Ki67 mRNA was observed in MSCs when engrafted in mouse wounds in combination with human untreated or ROT/AA-treated platelets on days 1 and 3 after the injury (Figure 2E).

As treatment with PRP has been reported to improve survival of MSCs exposed to oxidative stress (Hersant et al., 2019), we investigated whether transfer of platelet mitochondria was implied in this process. We examined the survival of human MSCs exposed to oxidative stress in the presence of human untreated or ROT/AA-treated platelets by flow cytometry following annexin V/7-aminoactinomycin D (7-AAD) staining. We found that both types of platelets exert the same efficacy in protecting damaged MSCs against cell death (Figure 2F and G) and that survival of damaged MSCs following platelet exposure was not affected in presence of 0.4 μm -pore size TW plates (Figure 2H). In agreement with *in vitro* observations, we noticed a greater survival of engrafted MSCs in mouse wounds when delivered in combination with platelets at day 1 post-injury with no significant difference between untreated and ROT/AA-treated platelets. However, on day 3 post-injury, improved survival of MSCs was found for mice grafted with MSCs in combination with untreated platelets compared to animals grafted with MSCs combined with ROT/AA-treated platelets (Figure 2I).

Platelet-derived respiration-competent mitochondria stimulate pro-angiogenic potential of MSCs.

As we have previously shown that PRP stimulates the pro-angiogenic properties of MSCs (Hersant et al., 2019), we tested whether platelet-derived mitochondria play a role in this process. We examined expression of vascular endothelial growth factor (VEGF) and hepatocyte growth factor (HGF) mRNA and secretion of the proteins by MSCs following their 24-h incubation to untreated platelets. We found that the mRNA of both cytokines was higher and their secretion was greater when MSCs were incubated with untreated but not with ROT/AA-treated platelets, in a dose-dependent fashion (Figure 3A and B). In addition, no cytokine secretion activation was found in MSCs incubated with platelets when platelet's mitochondria transfer was significantly reduced through the presence of 0.4 μm -pore size TW insert or treatment with dynasore (Figure 3C and D). In agreement with these observations, we found that VEGF and HGF secretion was higher when MSCs were exposed to mitochondria isolated from intact platelets but not from ROT/AA-treated platelets (Figure 3E). Overall, these findings indicate that transfer of respiration-competent platelet-derived mitochondria improve the angiogenic potential of MSCs.

Consistent with *in vitro* observations, we found that transcription of human VEGF and HGF was greater in human MSCs engrafted together with human untreated platelets in mouse wounds on days 1 and 3 post-injury compared to MSCs alone (Figure 3F). However, such

activation did not occur in case of ROT/AA-treated platelets (Figure 3F). The impaired capacity of human ROT/AA-treated platelets to stimulate the pro-angiogenic function of human MSCs *in vivo* was further confirmed via analysis of the wound vascularization using CD31 immunohistochemistry. Thus, on days 3 and 7 post-injury, a significantly higher number of endothelial cells were detected in the wounds treated with MSCs together with untreated platelets compared to MSCs alone or to MSCs combined with ROT/AA-treated platelets (Figure 3G and H). We also observed that transcription of angiogenesis-related host (murine) genes including CD31, vascular endothelial cadherin (VE-cadherin) and VEGF was more elevated in wounds injected with MSCs with untreated platelets compared to MSCs either alone or in combination with ROT/AA-treated platelets (Supplementary Figure 3 A and B).

Next, we examined whether platelet-derived mitochondria also improve the angiogenic potential of MSCs in an unrelated animal models of tissue injury. MSCs alone or in combination with intact platelets as well as MSCs preconditioned with intact isolated mitochondria were grafted in the tibialis anterior (TA) muscle of dystrophic α -sarcoglycan ($Scga^{null}$)-deficient mice. In this autosomal recessive limb-girdle muscular dystrophy type 2D model of chronic muscle injury, we found that human VEGF and HGF transcripts were higher in mouse TA grafted with human MSCs either together with intact human platelets or following their 'preconditioning' with isolated mitochondria on day 3 post-injury compared to TA treated with MSCs alone (Supplementary Figure 4A and B). Similarly, transcription of murine angiogenesis-related genes including CD31, VE-cadherin and VEGF and mouse myogenic desmin gene was elevated in mouse TA grafted with MSCs either with control platelets or following their 'preconditioning' with intact mitochondria suggesting that both angiogenesis and myogenesis processes were improved (Supplementary Figure 4C-F).

Platelet mitochondria stimulate pro-angiogenic activity of MSCs without altering their energetic status.

Given that mitochondria are a major contributor to cellular bioenergetics and adenosine triphosphate (ATP) production via oxidative phosphorylation, we investigated whether transport of mitochondria from platelets to MSCs stimulate their pro-angiogenesis activity via promotion of ATP generation. Prior to evaluation of the oxygen concentration rate (OCR) of MSCs following 24 h-exposure to untreated and ROT/AA-treated platelets, MSCs were washed to remove platelets. We then assessed basal respiration and proton leak, as well as non-mitochondrial respiration as described previously (Ryall, 2017). Consistent with the

import and requirement of respiration-competent mitochondria from platelets, exposure to untreated platelets was found to enhance respiration in MSCs, which was abolished when platelets were pre-treated with ROT/AA (Figure 4A and B). In addition, we estimated the cellular glycolytic activity by assessing the extracellular acidification rate (ECAR). Increase of ECAR was found for MSCs following their incubation with both untreated and ROT/AA-treated platelets (Figure 4C). However, exposure of MSCs to ROT/AA-treated platelets rendered the cells more glycolytic than their exposure to untreated platelets (Figure 4C). This metabolic shift to glycolysis is further supported by a decrease of OCR/ECAR ratio (Figure 4D), an increase of cellular levels of lactate (Figure 4E), and lactate dehydrogenase A (LDHA) mRNA (Figure 4F) and a decrease of the pyruvate/lactate ratio (Figure 4G) in MSCs exposed to ROT/AA-treated platelets. Finally, incubation of MSCs with both untreated and ROT/AA-treated platelets led to ATP content increase (Figure 4H) but did not alter their adenylate energy charge (Figure 4I).

Platelet mitochondria stimulate angiogenesis via activation of the *de novo* fatty acid synthesis in MSCs.

Given that high adenylate energy charge (>0.8) favors anabolic reactions, such as citrate cleavage (Atkinson and Walton, 1967; De la Fuente et al., 2014; Shen et al., 1968), we reasoned that exceeding energy production by platelet mitochondria may promote angiogenesis by means of anabolic processes. As *de novo* fatty acid synthesis was previously reported to promote angiogenesis in endothelial and cancer cells (Bruning et al., 2018; Röhrig and Schulze, 2016), we examined whether this metabolic pathway is activated in MSCs following their incubation with untreated or ROT/AA-treated platelets. We first analyzed levels of key enzymes of *de novo* fatty acid synthesis including ACLY, ACC and FAS. We found that incubation of human MSCs with human untreated platelets increased expression of the 3 enzymes at both mRNA and protein levels in a concentration-dependent fashion (Figure 5A and B). However, this activation was abolished when MSCs were incubated with ROT/AA-treated platelets. Similarly, in mouse wounds on days 1 and 3 post-injury, human MSCs expressed higher levels of ACC and FAS when engrafted in combination with human platelets compared to MSCs alone (Figure 5C). Again, this upregulation did not occur in MSCs when grafted with ROT/AA-treated platelets.

To determine whether stimulation of fatty acid synthesis is involved in the pro-angiogenic effects exerted by platelets on MSCs, we performed ELISA assays to assess the level of secreted VEGF and HGF by MSCs following their incubation with platelets in the

presence of C75, a pharmacological inhibitor of FAS. We found that inhibition of FAS completely abrogated secretion of VEGF and HGF promoted by incubation of MSCs with platelets (Figure 5D). Additionally, C75 had no effect on platelet-enhanced proliferation of MSCs (Figure 5E), corroborating our previous observations that this process is independent of transfer of mitochondria from platelets to MSCs.

Transfer of platelet-derived mitochondria to MSCs activates citrate-dependent fatty acid synthesis via stimulation of the TCA cycle.

To identify the metabolic pathways involved in the pro-angiogenic activity of MSCs due to transfer of mitochondria from platelets using unbiased approach, we performed non-targeted large-scale metabolomic analysis of MSCs following their incubation with untreated or ROT/AA-treated platelets. A panel of 81 metabolites (mainly from the TCA cycle, fatty and amino acid glycolysis, purine metabolism and the pentose phosphate pathway) was identified and used to construct a heat map-based unsupervised hierarchical clustering analysis (Figure 6A). Metabolomic profiling revealed that incubation of MSCs with untreated platelets induces metabolic remodeling (Figure 6A). These modifications were ascribed to the effect of platelet mitochondria on MSCs, since treatment of platelets with ROT/AA blunted these changes (Figure 6A). Integrative pathway analysis of these datasets using MetaboAnalyst (www.metaboanalyst.ca) revealed significant upregulation of citrate, pyruvate and metabolites of fatty acid synthesis and amino acid synthesis pathways (Supplementary Figure 5A). Indeed, fatty acid metabolites (including arachidonic acid, linoleic acid, palmitic acid, pantothenic acid, stearic acid and cholesterol) and metabolites linked to the TCA cycle (including 2-hydroxyglutarate, 2-oxoglutarate, aspartate, citrate, GABA, glutamate and malate), were significantly increased in MSCs incubated with untreated platelets, and this effect was abrogated when platelets were pre-treated with ROT/AA (Figure 6B and C). A similar trend was also observed for amino acids; but these differences were mostly not significant (Supplementary Figure 5B).

We next performed associated pathway analysis, localization and enzymatic function enrichment to further characterize the effects of platelets. The results indicate that metabolic modifications induced in MSCs by platelets are specific for the mitochondrial compartment (Supplementary Figure 5C). This analysis also identifies that citrate exchange and fatty acid synthesis are greater in MSCs in response to incubation with platelets (Supplementary Figure 5C and D), suggesting that the effect of platelets is mediated by stimulation of citrate production that, in turn, activates fatty acid synthase (Williams and O'Neill, 2018). In

addition, we assessed citrate synthase activity in MSCs incubated with platelets, and found that the increase in the activity was abrogated when platelets were pre-treated with ROT/AA, and this effect was independent of citrate synthase mRNA level (Figure 6D and E). These experiments suggest that increased level of citrate in MSCs following their incubation with untreated platelets is promoted due to transfer of mitochondria from platelets to MSCs. Next, we performed metabolomic profiling of untreated and ROT/AA-treated platelets. Integrative pathway analysis of 115 metabolites revealed that ROT/AA treatment induced dysregulation of the metabolome characterized by efficient inhibition of the respiratory chain in platelets, inducing a metabolic shift toward glycolysis, indicative of the Warburg effect (Figure 6F and G). As expected, respiratory chain inhibition altered the TCA cycle (Figure 6F and G) and led to reduction in citrate level (Figure 6H).

Citrate restores the pro-angiogenic effects in MSCs incubated with ROT/AA-treated platelets.

To further assess the role of citrate levels promoted by platelet mitochondria in MSCs in the stimulation of fatty acid synthesis and angiogenesis potential of the cells, MSCs were incubated with ROT/AA-treated platelets in the presence of 10 mM citrate. Under this scenario, MSCs showed higher mRNA for fatty acid synthesis (ACLY, ACC, FAS) and angiogenic (VEGF and HGF) related genes (Figure 7A and B) and greater secretion of VEGF and HGF proteins (Figure C). In contrast, citrate treatment failed to improve the pro-angiogenic potential of intact platelets since similar levels of VEGF and HGF transcripts and VEGF protein were found in MSCs exposed to intact platelets both in the absence and presence of citrate (Figure 7D and E). These results suggest that in the presence of citrate, ROT/AA-treated platelets recover their ability to activate the fatty acid synthesis and angiogenesis potential in MSCs. Further, the presence of citrate did not alter the effects of ROT/AA-treated platelets on MSC proliferation (Figure 7F) while citrate inhibited the mitogenic potential of intact platelets (Figure 7G).

Consistent with these *in vitro* observations, we found that addition of citrate improved the wound-healing activity of human MSCs grafted together with human ROT/AA-treated platelets (Figure 7H and I). Addition of citrate was also found to stimulate transcription of human fatty acid synthesis (ACC and FAS) and human angiogenesis (VEGF and HGF)-related genes following engraftment of human MSCs together with human ROT/AA-treated platelets (Figure 7J). Finally, we found that wounds treated with human MSCs together with human ROT/AA- platelets in the presence of citrate exhibited higher re-vascularization on

days 3 and 7 post injury as assessed by the expression of mouse CD31, VE-cadherin and VEGF mRNA (Figure 7K).

DISCUSSION

Platelet preparations are widely used in clinical applications to promote wound healing and tissue regeneration or to optimize MSCs-based therapies (Kawase, 2015). Such clinical use is primarily based on the rationale that activated platelets released alpha-granules that contain high levels of growth factors (De Pascale et al., 2015; Etulain, 2018). Although the role of the soluble factors released by platelets in wound healing is undisputable, our study revisits the notion that platelets act by means of their paracrine secretion, focusing on the role of their respiration-competent mitochondria in stem cell-based therapy. The release of functional mitochondria by platelets following their activation has been reported for both *in vitro* and *in vivo* systems (Boudreau et al., 2014; Marcoux et al., 2017). Further, circulating cell-free respiratory competent mitochondria have also been detected in blood from healthy patients in normal physiological state (Al Amir Dache et al., 2020). However, the molecular mechanism and consequences of this phenomenon were not understood with only two studies describing that mitochondria released by activated platelets can be taken up by neutrophils or pancreatic β -islets, where they trigger immune or 'healing' responses, respectively (Boudreau et al., 2014; Zhao et al., 2017).

Consistent with the above reports, we document here that mitochondria released by activated platelets can be internalized by MSCs and that this process significantly improves the therapeutic efficacy of the stem cells after their grafting into mouse wounds. Although deeper investigations are needed, a strikingly similar phenomenon is occurring following combined delivery of MSCs with platelets in mouse dystrophic muscles.

Interestingly, our study indicates that platelet-derived mitochondria are primarily taken up by MSCs via dynamin-dependent endocytosis. A similar mechanism of endocytosis was initially reported by Islam and colleagues as mediating the transfer of mitochondria from engrafted MSCs to lipopolysaccharide- injured lung epithelial cells (Islam et al., 2012). However, in sharp contrast with these observations, we found that formation of connexin 43 gap junctions between MSCs and platelets is not required for the internalization of platelet mitochondria by MSCs. Therefore, our study points to another mechanism by which mitochondria can move between cells, apart from the described trafficking modalities that include endocytosis, macropinocytosis (Kitani et al., 2014; Patel et al., 2017), or tunneling nanotubes (Rodriguez et al., 2018) involving the kinesin mobility system (Henrichs et al.,

2020). It thus seems that the transfer of mitochondria is a general phenomenon with relevance in wound healing, inflammation, cancer (Berridge et al., 2016; Nakhle et al., 2020; Rodriguez et al., 2018) and beyond, but the underlying molecular machinery may change based on the cell types relevant in a given (patho-) physiological scenario. For example to trigger adaptive repair response to cell and tissue injury, mitochondria from apoptotic cells are preferentially transferred to MSCs through tunneling nanotubes (Figeac et al., 2014; Mahrouf-Yorgov et al., 2017) while mitochondria from activated platelets are shown here, to be internalized via endocytosis.

Given that platelet mitochondria need to have functional respiration to enhance the therapeutic efficacy of MSCs, we wondered by what mechanism respiration-competent mitochondria from platelets taken up by MSCs modulate their wound-healing activity. In support of this supposition, activated platelets have been reported to potentiate several important properties in MSCs, which include their proliferation, survival and angiogenic potential (Hersant et al., 2019). Indeed, our findings unequivocally show that platelet-derived respiration-competent mitochondria contribute to the enhancement of the angiogenic potential of the recipient MSCs, while they do not affect their proliferation or survival. These observations support the notion that platelets exert their cytoprotective and mitogenic effects on MSCs via the release of mitogenic growth factors as previously reported by several groups (Lai et al., 2018; Rodrigues et al., 2010), rather than by mitochondria transfer to MSCs.

Interestingly, our data indicate that platelet mitochondria enhance the angiogenic activity of the recipient MSCs by reprogramming their metabolism. In particular, we show that mitochondria derived from platelets activate the TCA cycle in the recipient MSCs, resulting in the increase of several metabolites. Of particular interest is citrate that has been critically implicated in the pro- angiogenic process (Binu et al., 2013).

The fact that citrate failed to accumulate in MSCs following their incubation with platelets with suppressed mitochondrial respiration may be a direct consequence of the inhibition of complex I-NADH-dehydrogenase activity in platelet mitochondria. This results in accumulation of NADH that, in turn, inhibits the TCA cycle enzymes including isocitrate dehydrogenase and α -ketoglutarate dehydrogenase (Berg et al., 2002; Hull and Whereat, 1967). Citrate supplied by TCA cycle of platelet-derived mitochondria is likely exported to the cytosol of recipient MSCs, where it fuels the ACLY enzyme that initiates fatty acid synthesis. The citrate-dependent stimulation of fatty acid synthesis to sustain pro-angiogenic effects of platelets is further demonstrated by the restoration of wound healing properties of platelets with suppressed respiration by exogenous citrate. Our experiments with C75, an

inhibitor of FAS, strongly indicate that *de novo* fatty acid synthesis is required for the stimulation of angiogenesis by MSCs, probably due to the provision of building blocks for membrane formation linked to the secretion of paracrine factors that promote the process of angiogenesis. Our results are corroborated by previous reports revealing that aberrant overexpression of several key enzymes of the fatty acids synthesis pathway in various cancer types correlated with enhanced angiogenesis (Duan et al., 2017; Menendez and Lupu, 2017; Pope et al., 2019). However, the molecular mechanism underlying the link between fatty acids and angiogenesis has not been investigated in this study.

Recent work has documented that inhibition of FAS results in accumulation of malonyl-CoA, causing mTOR malonylation with ensuing inhibition of angiogenesis (Bruning et al., 2018). In the context of our study, we hypothesized that activation of fatty acid synthesis reduces mTOR malonylation and thus reduces its inhibitory effect on angiogenesis, whereby allowing for this process to proceed. In addition, there are reports showing that aberrant TCA cycle stoichiometry or fatty acids content promotes genetic reprogramming via modification of epigenetic processes (Martínez-Reyes and Chandel, 2020; McDonnell et al., 2016). Therefore, accumulation of citrate and fatty acids in MSCs in response to incubation with platelets promotes expression and secretion of pro-angiogenic factors, as previously reported for endothelial or cancer cells (Binu et al., 2013; Bruning et al., 2018; Frezza, 2017; Zhou et al., 2016).

Our research on the role of platelet mitochondria in activating the pro-angiogenic activity of MSCs is a new example how intercellular transfer of mitochondria modifies the behavior of recipient cells. There are studies documenting the existence of intercellular mitochondria transfer involving several cell types both *in vitro* and *in vivo* approaches (Acquistapace et al., 2011; Islam et al., 2012; Li et al., 2016; Liu et al., 2014; Rodriguez et al., 2018). Most of the studies in this field focused on mitochondrial transfer from donor cells (most likely MSCs) to damaged cells or cancer cells as a process improving their survival (Acquistapace et al., 2011; Islam et al., 2012; Li et al., 2016; Liu et al., 2014; Rodriguez et al., 2018), chemoresistance (Caicedo et al., 2015; Dong et al., 2017; Tan et al., 2015; Rodriguez et al., 2018) or function (Tan et al., 2015; Dong et al., 2017; (Henrichs et al., 2020). In contrast, the consequences of mitochondria transferred to MSCs are much less documented with only few studies suggesting that this phenomenon may be implied in differentiation of stem cells and in activation of their anti-apoptotic function (Koyanagi et al., 2005; Mahrouf-Yorgov et al., 2017). The various effects of mitochondrial transfer in recipient cells are likely dependent on the type of donor cells as well as their physiological state (Nakhle et al., 2020;

Rodriguez et al., 2018). From this point of view, mitochondria of platelets are likely to differ from these organelles in other cells, as platelets are devoid of mitochondrial biogenesis due to the lack of a nucleus and are packaged into platelets during their formation from megakaryocytes (Melchinger et al., 2019).

Future investigations will be required to fully characterize the role of mitochondria released by platelets under physiological conditions and to understand whether these organelles convey the pro-healing effects of platelets *in vivo*. It is of particular interest to elucidate the cell types that internalize mitochondria released by platelets *in vivo*, for instance in the context of tissue injury and the consequences of this phenomenon in the activation of the endogenous tissue repair processes. In particular, it is of high importance to determine if the effectiveness of endogenous MSCs or progenitors cells in wound repair is conditioned by the proximity of platelets and their activation in response to tissue injury. In this regard, our study documents that mitochondria are important mediators of the pro-healing effects of platelets on MSCs and corroborates the notion that to use platelet preparations (in regenerative medicine, the quality and functionality of platelet mitochondria ought to be taken into consideration.

LIMITATIONS OF STUDY

While our study highlights that platelet-derived mitochondria are transferred to MSCs, observation of this phenomenon by transmission electron microscopy presents technical limitations. For example, it is unclear if the imaged structure of platelet-derived mitochondria in the extracellular medium is correctly preserved and subtle structural differences between mitochondria from intact or ROT/AA-treated platelets are not overlooked. In addition, we have shown that platelet-derived mitochondria stimulate mitochondrial fusion in recipient MSCs, but we do not know if platelet mitochondria are incorporated into the fused mitochondrial network. It is also unclear how ROT/AA-treated platelets trigger a metabolic shift toward glycolysis in MSCs.

DECLARATION OF INTERESTS

The authors declare that they have no competing interests.

AUTHOR CONTRIBUTIONS

JL performed most of *in vitro* experiments. AP interpreted metabolomics studies and helped in writing the manuscript. PL performed most of the *in vivo* experiments. MG performed confocal microscopy experiments. NC performed bone formation experiments. ZK and KF performed *in vivo* experiments in mouse skeletal muscles. SBL performed *in vitro* angiogenesis ELISA, LB performed Seahorse experiments, ASc and AY performed transmission electron microscopy experiments, AS and BH helped in *in vivo* experiments. MSA helped in *in vitro* experiments. JR, KK and JN provided C57BL/6J^{su9-DsRed2} mice and helped with the design of experiments. FR helped with the design of experiments. AMR designed the research and wrote the manuscript. All authors helped with editing of the manuscript.

ACKNOWLEDGEMENTS

We thank Sylvère Durand and the metabolomic platform of the Institut Gustave Roussy (AMMICa US23/CNRS UMS3655) for metabolomic analysis. We thank the transmission electron microscopy platform of Cochin Institute (INSERM/CNRS, Paris). We thank Aurélie Guguin and Adelyne Henry and the flow cytometry platform of Mondor Institute for Biomedical Research (INSERM U955, Créteil). We thank Hadrien Chauvin (EnvA, Maisons-Alfort, France) for assistance in statistical analysis. We thank Prof. Okabe for providing the CAG/su9-DsRed2 plasmid, and the Transgenic Unit, Institute of Molecular Genetics, CAS, Prague, Czech Republic, for production of transgenic mouse founders. We thank Prof. Mark Forwood (School of Medical Science of Griffith University, Australia) and Prof Mike Berridge (Malaghan University, New Zealand) for the critical reading of the manuscript and their suggestion to improve it. This work was supported by Fondation des Gueules Cassées, Association Neurofibromatoses et Recklinghausen and Fondation de l'Avenir (AP-RM-19-001) (AMR), Association Française contre les Myopathies (AFM) via TRANSLAMUSCLE (PROJECT 19507) (FR), and by the 7th Framework Program of the European Commission (project REBORNE no. 241879) (NC), from the Czech Science Foundation 20-18513S (JR), 18-10832N and 20-05942S (both JN), and the Czech Health Foundation NU20-03-00309 (KK), 17-30138A (JN).

FIGURE LEGENDS

Figure 1: Mitochondria released by platelets stimulate wound-healing activity of MSCs.

(A) Representative confocal microscopy pictures of human MSCs after 24 h incubation with human intact platelets or human platelets following exposure to ROT/AA and previously labelled with Mitotracker Green (green signal) ($n = 6$), or with mouse intact or ROT/AA-treated platelets isolated from C57BL/6J^{su9-DsRed2} mice (red signal) ($n = 6$), to identify platelet-derived mitochondria. Left panels, Mitotracker green fluorescence of untreated MSCs. WGA, wheat germ agglutinin (white signal). Scale bars: 20 μm .

(B) Representative flow cytometry histogram of internalization of Mitotracker Green-labelled mitochondria from human platelets (left panel, red line) ($n = 6$) or DsRed fluorescent mitochondria isolated from C57BL/6J^{su9-DsRed2} mouse platelets ($n = 5$) by MSCs (right panel, red line). Gray histograms, untreated MSCs.

(C) Flow cytometry quantification of transfer of mitochondria from Mitotracker Green-labelled human platelets to MSCs following their 24 h incubation with different numbers ([Plts 1], [Plts 2], [Plts 3]) of platelets ($n \geq 6$).

(D) Representative flow cytometry histogram of internalization by MSCs of Mitotracker Green-labelled mitochondria from human untreated platelets in the presence of TW inserts (left panel, red line) ($n = 5$) or from human ROT/AA-treated platelets (right panel, red line) ($n = 5$). Blue line, MSCs exposed to human untreated platelets. Gray histograms, untreated MSCs.

(E) Flow cytometry quantification of platelet-derived mitochondria in MSCs after 24 h incubation with different number ([Plts 1], [Plts 2] and [Plts 3]) of human untreated platelets in the presence of TW insert ($n \geq 5$) or with ROT/AA-treated platelets ($n \geq 5$) relative to MSCs incubated with human untreated platelets.

(F) Representative photographs of mouse back with skin wounds on day 7 following injury and their treatment with either saline solution, human untreated platelets, human ROT/AA-treated platelets, human MSCs alone or human MSCs in combination with human untreated or ROT/AA-treated platelets ($n = 10$).

(G) Closure of wounds exposed to different conditions on days 3 and 7 following the injury ($n = 10$).

Platelets were used at a concentration of 8×10^7 /mL medium in (A), (B), (D), (F) and (G). [Plts 1], [Plts 2] and [Plts 3] correspond to 2×10^7 , 4×10^7 or 8×10^7 platelets/mL, respectively. One way Anova with Dunn's multiple comparisons test in (C) and (E). One way Anova with Tukey's multiple comparisons test in (G). * $P < 0.05$, ** $P < 0.01$, *** $P < 0.001$, **** $P < 0.0001$. Each dot represents an independent experiment in (C, E)) or a single mouse in (G). Bar graphs represent mean \pm SD

Figure 2. Platelet-derived mitochondria are not involved in proliferative and cytoprotective effects of platelets on MSCs.

(A) Representative flow cytometry histograms (left panels, red line) and relative flow cytometry quantification (right panel) of CFSE staining of human MSCs following 24-h incubation with different concentrations ([Plts 1], [Plts 2] and [Plts 3]) of human untreated or ROT/AA-treated platelets compared to MSCs alone ($n \geq 5$). Gray histograms (left panels), MSCs alone

(B-D) Relative Ki67 mRNA level in human MSCs after 24-h incubation with (B) different numbers ([Plts 1], [Plts 2] and [Plts 3]) of human untreated or ROT/AA-treated platelets compared to MSCs alone ($n \geq 6$), (C) human untreated platelets in absence or presence of TW inserts compared to MSCs alone ($n = 4$) or (D) human untreated platelets in presence of dynasore by comparison to untreated or dynasore-treated MSCs ($n = 3$).

(E) Relative human Ki67 mRNA level in mouse wounds grafted with human MSCs in combination with human untreated or ROT/AA-treated platelets compared to MSCs grafted alone, on day 1 ($n \geq 5$) and day 3 ($n = 6$) after the injury.

(F) Representative flow cytometry dot blots for annexin V/7AAD staining of H_2O_2 -exposed human MSCs grown alone or following 24-h exposure to human untreated or ROT/AA-treated platelets ($n = 7$). Bottom- right quadrants, % viable cells; upper-right quadrant, % necrotic cells; bottom-left quadrant; % early apoptotic cells; upper-left quadrant, % late apoptotic cells

(G-H) Relative survival of H₂O₂-injured human MSCs after their exposure (G) to different number ([Plts 1], [Plts 2] and [Plts 3]) of human untreated or ROT/AA-treated platelets ($n \geq 6$) or (H) to human untreated platelets in the absence or presence of TW inserts ($n = 10$) compared to MSCs alone.

(I) Relative survival of human MSCs engrafted in combination with human untreated or ROT/AA-treated platelets in mouse wounds related to MSCs grafted alone, assessed by quantitative analysis of human TBP mRNA, on day 1 ($n \geq 7$) and day 3 ($n = 9$) post-injury.

Platelets were used at 8×10^7 /mL in (A, left panels), (C-F) and (H-I).

[Plts 1], [Plts 2] and [Plts 3] correspond to 2×10^7 , 4×10^7 or 8×10^7 platelets/mL, respectively. One way Anova with Dunn's multiple comparisons test in (A-E) and (G-I). * $P < 0.05$, ** $P < 0.01$, *** $P < 0.001$. Each dot represents an independent experiment in (A-D) and (G-H) or a single mouse in (E) and (I). Bar graphs represent mean \pm SD.

Figure 3. Platelet-derived mitochondria stimulate pro-angiogenic properties of MSCs.

(A-B) Relative mRNA ($n \geq 4$) (A) and protein levels of VEGF and HGF ($n \geq 5$) (B) in conditioned media from MSCs following 24-h incubation with different numbers ([Plts 1], [Plts 2] and [Plts 3]) of untreated and ROT/AA-treated platelets relative to MSCs grown alone.

(C-E) Relative protein levels of VEGF and HGF in conditioned media from human MSCs following 24 h incubation with (C) human untreated platelets in the absence or presence of TW insert relative to MSCs grown alone (untreated) ($n \geq 5$), (D) human untreated platelets in presence of dynasore by reference to dynasore-treated MSCs grown alone ($n = 5$) or (E) isolated mitochondria from human intact or ROT/AA-treated platelets relative to MSCs grown alone ($n = 4$).

(F) Relative level of human VEGF and human HGF mRNA in mouse wounds grafted with human MSCs in combination with human untreated or ROT/AA-treated platelets related to MSCs engrafted alone, on day 1 ($n \geq 6$) and day 3 ($n \geq 5$) post-injury.

(G-H) Representative CD31 immunostaining (red signal) at day 3 post-injury (Hoechst 33342 blue signal, nuclei; scale bar, 50 μm) (G) and CD31 immunostaining quantification of mouse wounds at day 3 ($n = 5$) and day 7 ($n \geq 5$) (H), following treatment with saline solution, human intact platelets, human ROT/AA-treated platelets, human MSCs, or human MSCs in combination with either human intact or ROT/AA-pretreated platelets, respectively.

[Plts 1], [Plts 2] and [Plts 3] correspond to 2×10^7 , 4×10^7 or 8×10^7 platelets/mL, respectively. One way Anova with Dunn's multiple comparisons test in (A-E). Unpaired Student t-test in (D). * $P < 0.05$, ** $P < 0.01$, *** $P < 0.001$, **** $P < 0.0001$. Each dot represents an independent experiment in (A-D) and (G-H) or a single mouse in (F) and (H). Bar graphs represent mean \pm SD.

Figure 4. Platelet-derived mitochondria do not alter the energetic status of MSCs.

(A) OCR assessed in human MSCs cultivated alone or in the presence of human untreated or ROT/AA-treated platelets. After the evaluation of basal respiration, oligomycin (O), FCCP (F) and rotenone/antimycin A (ROT/AA) were added as shown ($n = 8$).

(B) Basal respiration, ATP-linked respiration, proton leak, and maximal respiration of human MSCs cultivated alone or in the presence of human untreated or ROT/AA-treated platelets ($n = 8$).

(C-D) ECAR ($n = 8$) (C) and OCR/ECAR ratio ($n = 8$) (D), for MSCs incubated with untreated or ROT/AA-treated platelets compared to untreated MSCs.

(E-G) Relative lactate level ($n = 4$) (E), relative level of LDHA mRNA ($n = 8$) (F) and, pyruvate/lactate ratio presented in log₂ ratio ($n = 3$) (G), in MSCs incubated with untreated or ROT/AA-treated platelets compared to untreated MSCs.

(H-I) Relative ATP level ($n \geq 4$) (H) and relative adenylate energy charge ($n = 3$) (I), for MSCs incubated with untreated or ROT/AA-treated platelets compared to untreated MSCs.

Platelets were used at 8×10^7 /mL in (A-I). Welch's Anova followed by Welch's t test in (B-D). One way Anova with Dunn's multiple comparisons test in (E) and (G-I). One-way ANOVA followed by Tukey's multiple comparisons test in (F). * $P < 0.05$, ** $P < 0.01$, *** $P < 0.001$

and **** $P < 0.0001$. Each dot represents an independent experiment. Bar graphs represent mean \pm SD.

Figure 5. Platelet-derived mitochondria stimulate angiogenesis via activation of *de novo* fatty acid synthesis in MSCs.

(A) Relative levels of ACLY ($n \geq 3$), ACC ($n \geq 6$) and FAS ($n \geq 6$) mRNA in human MSCs after 24-h incubation with different numbers ([Plts 1], [Plts 2] and [Plts 3]) of human untreated or ROT/AA-treated platelets compared to MSCs incubated alone.

(B) Immunocytochemistry of ACLY, ACC and FAS proteins (red signal) in human MSCs grown alone or incubated in the presence of human untreated or ROT/AA-treated platelets ($n = 4$). Blue signal, Hoechst 33342 stained nuclei; scale bars, 50 μm .

(C) Human ACC and human FAS mRNA level in mouse wounds engrafted with human MSCs in combination with human untreated or ROT/AA-treated platelets relative to MSCs grafted alone, on days 1 and 3 post-injury ($n \geq 5$).

(D) Level of VEGF and HGF proteins in conditioned media from human MSCs after 24-h incubation with different numbers ([Plts 1], [Plts 2] and [Plts 3]) of human platelets in the absence or presence of C75 relative to MSCs alone or C75-exposed MSCs, respectively ($n \geq 4$).

(E) Level of Ki67 mRNA in human MSCs after 24-h exposure to different numbers ([Plts 1], [Plts 2] and [Plts 3]) of human platelets in the presence of C75 relative to MSCs incubated alone or treated with C75, respectively ($n \geq 5$).

[Plts 1], [Plts 2] and [Plts 3] correspond to 2×10^7 , 4×10^7 or 8×10^7 platelets/mL, respectively. Human platelets were used at 8×10^7 /mL in (B) and (C). One way Anova with Dunn's multiple comparisons test in (A) and (C-E). * $P < 0.05$, ** $P < 0.01$, *** $P < 0.001$, **** $P < 0.0001$. Each dot represents an independent experiment in (A), (D) and (E) or a single mouse in (C). Bar graphs represent mean \pm SD.

Figure 6. Platelet mitochondria stimulate citrate-dependent fatty acid synthesis in MSCs.

(A) Heat-map of relative abundance of 81 metabolites (rows) in MSCs incubated alone or in the presence of intact or ROT/AA-treated platelets. Each column represents an individual sample ($n = 3$).

(B-C) Dot plots of relative abundance of (B) fatty acid metabolites ($n = 3$) and (C) TCA cycle-associated metabolites ($n = 3$) in human MSCs cultivated alone or with human untreated or ROT/AA-treated platelets.

(D-E) Relative citrate synthase (CS) mRNA level ($n \geq 6$) (D), and enzymatic activity ($n = 8$) (E), in human MSCs cultivated alone or with human untreated or ROT/AA-treated platelets.

(F-G) Integrative pathway (F) and enrichment analysis (G) using MetaboAnalyst of dysregulated metabolites in human platelets treated with ROT/AA compared to untreated platelets ($n = 3$)

(H) Citrate content in human untreated or ROT/AA-treated platelets ($n = 3$).

Human platelets were used at 8×10^7 /mL in (A-F). One-way ANOVA on rank followed by Conover-Iman pairwise comparisons with Benjamini-Hochberg P -values in (B) and (C). One way Anova with Dunn's multiple comparisons test in (D) and (E). Unpaired Student t-test in (H). * $P < 0.05$, ** $P < 0.01$. Each dot represents an independent experiment in (A-E) and (H). Bar graphs represent mean \pm SD

Figure 7. Citrate restores the pro-angiogenic effects in MSCs incubated with ROT/AA-treated platelets.

(A-C) Relative level of ACLY, ACC and FAS mRNA ($n \geq 4$) (A), VEGF and HGF mRNA ($n \geq 5$) (B) and, secreted VEGF and HGF proteins (C), in human MSCs after 24-h exposure to 10 mM citrate or human ROT/AA-treated platelets in the absence or presence of 10 mM citrate relative to MSCs incubated alone ($n \geq 6$).

(D) Relative level of VEGF and HGF mRNA in human MSCs after 24-h exposure to human intact platelets in absence or presence of 10 mM citrate relative to MSCs incubated alone ($n \geq 5$).

(E) Relative level of secreted VEGF protein in human MSCs after 24-h exposure to 10 mM citrate or human intact platelets in the absence or presence of 10 mM citrate relative to MSCs incubated alone ($n \geq 5$).

(F-G) Ki67 mRNA in human MSCs after 24-h exposure to (F) 10 mM citrate or human ROT/AA-treated platelets in the absence or presence of 10 mM citrate relative to MSCs incubated alone ($n \geq 6$) or (G) human intact platelets in presence of 10 mM citrate relative to MSCs incubated with intact platelets in absence of citrate ($n = 6$).

(H-I) Representative photographs of mouse back with skin wounds on day 7 post- injury ($n = 6$) (H) and closure rates of wounds on days 3 and 7 post-surgery ($n \geq 6$) (I), following their treatment with either human MSCs), MSCs plus 10 mM citrate, MSC in combination with human ROT/AA-treated platelets or MSC in combination with ROT/AA-treated platelets and 10mM citrate.

(J-K) Relative level of human ACC, FAS, VEGF and HGF mRNA in mouse wounds assessed in human MSCs grafted in the presence of 10 mM citrate or human MSCs grafted together with human ROT/AA-treated platelets in the absence or presence of 10 mM citrate relative to MSCs grafted alone, on day 3 post-injury ($n \geq 6$).

(K) Relative levels of mouse CD31, VE-cadherin and VEGF in the different groups on days 3 and 7 post-surgery ($n \geq 6$).

Platelets were used at 8×10^7 /mL in (A-K). One way Anova with Dunn's multiple comparisons test in (A), (C), (E-F) and (I-K). One way Anova with Tukey's multiple comparisons test in (B). Unpaired Student t-test in (D) and (G). * $P < 0.05$, ** $P < 0.01$, *** $P < 0.001$, **** $P < 0.0001$. Each dot represents an independent experiment in (A-D) and (G-H) or a single mouse in (F) and (H). Bar graphs represent mean \pm SD..

STAR METHODS

RESOURCE AVAILABILITY

Lead Contact

Further information and requests for resources and reagents should be directed to and will be fulfilled by the Lead Contact, Anne-Marie Rodriguez (anne-marie.rodriguez@inserm.fr).

Materials Availability

This study did not generate new unique reagents.

Data and Code Availability

This study did not generate any unique datasets or code.

EXPERIMENTAL MODEL AND SUBJECT DETAILS

Mouse strains

Mouse lines used in this study have been described and provided by the corresponding laboratories: C57BL/6JRj mice (Janvier Laboratories, Cat#2670020, RRID: MGI:2670020), SCID mice (Charles River Laboratories). C57BL/6J^{su9-dsRed2} mice were generated in the Transgenic Unit of the Czech Centre for Phenogenomics (CCP), Institute of Molecular Genetics, Prague, Czech Republic and sgca^{null} mice were generated in the University of Iowa College of Medicine, Iowa, United States (see below).

The animals were housed five or two per cage prior to and after the surgery, respectively in cages containing litter and refinement elements such as a plastic house and cotton for nest making and were allowed food and water *ad libitum*. They were in a temperature-controlled (22°C) animal facility with a 12-hour light/dark cycle. The general health of the mice was monitored daily for any signs of suffering or abnormal behavior. We used 8-week-old males to avoid potential interference from female hormones in the interpretation of our results. Sgca^{null} mice were the result of in-house breeding and C57Bl6/J mice were imported from the supplier and used after one week of acclimatization prior to the procedure.

Generation of C57BL/6J^{su9-dsRed2} mice

Transgenic reporter mice expressing red fluorescent protein in somatic cell mitochondria (harboring the CAG/su9-DsRed2 transgene) were generated in the Transgenic Unit of the Czech Centre for Phenogenomics (CCP), Institute of Molecular Genetics, Prague, Czech

Republic, using a pronuclear injection of the construct provided by Prof. Masaru Okabe (Osaka University, Japan) (Hasuwa et al., 2010) in C57BL/6J mice. The C57BL/6J^{su9-dsRed2} mice are property of the Laboratory of Reproductive Biology, Institute of Biotechnology, Czech Academy of Sciences, Vestec, Czech Republic. The stable colony of transgenic mice is housed in the CCP (Animal Ethics Number 66866/2015-MZE-17214, approved December 18, 2015).

Generation of $sgca^{null}$ mice

Transgenic mice lacking the alpha sarcoglycan expression ($sgca^{null}$) were generated at the University of Iowa College of Medicine, Iowa, United States (Duclos et al. 1998). Briefly, a linearized construct (replacing exon 2, exon 3, 571 bp of intron 1 and 65 bp of intron 3 with a neomycin resistance gene, in the opposite transcriptional orientation) was electroporated into ES cells. C57BL/6J blastocysts were then microinjected with cells from correctly targeted clones. The mice were on a C57BL6/N and J mixed background and crossed as homozygous.

hMADS cells

All experiments were conducted using human multipotent adipose-derived stem (hMADS) cells as a model of human MSCs. These cells can be maintained in culture for some 200 population doublings with apparently unchanged phenotype. hMADS cells were isolated from adipose tissues obtained from young donors after informed parental consent as previously reported (Rodriguez et al., 2005). Adipose tissue from young children was obtained with the informed consent of the parents as surgical scraps from surgical specimen of various surgeries, as by the Comité de Protection des Personnes, Centre Hospitalier Universitaire de Nice in 2001 and Comité de Protection des Personnes, Centre Hospitalier Universitaire de Créteil in 2007. hMADS cells were cultured in Dulbecco's modified Eagle's medium (DMEM, Gibco, Cat# 21885025) supplemented with 1 g/L glucose, 10% heat-inactivated fetal bovine serum (FBS) (Dominique Dutscher, Cat#S1810-500), 100 U/mL penicillin, 100 µg/mL streptomycin, and 10 mM HEPES (Gibco, Cat#15630056). As described earlier (Rodriguez et al., 2005), hMADS cells exhibited the following phenotype: CD44⁺, CD49b⁺, CD105⁺, CD90⁺, CD13⁺, Stro-1⁻, CD34⁻, CD15⁻, CD117⁻, Flk-1⁻, Gly-A⁻, CD133⁻, HLA-DR⁻ and HLA-I^{low}. hMADS cells were maintained in a 5 % CO₂ atmosphere at 37 °C. For *in vitro* studies, MSCs were pre-incubated for 24 h with FBS-free DMEM culture medium supplemented with heparine (20 U/mL) and containing platelets at 2x10⁷/mL, 4x10⁷/mL or 8x10⁷/mL medium.

For some experiments, human MSCs were co-cultivated with platelets in presence of cell culture insert (Transwell) containing polycarbonate membrane of 0.4 μ m pore size (Millicell, Millipore, Cat#PIHP03050). Under this setting, MSCs were seeded in the bottom compartment of the well. To inhibit fatty acid synthase, MSCs were treated with 5 mg/mL C75 (Sigma-Aldrich, Cat#C5490) for 24 h in serum free culture medium alone or in the presence of various concentrations of platelets. To assess the role of platelet's citrate, MSCs were exposed to ROT/AA-pretreated platelets in the presence of 10 mM sodium citrate tribasic dihydrate (Sigma-Aldrich, Cat#S4641).

METHOD DETAILS

Platelet preparation and inhibition of mitochondrial respiration

Human platelet-rich plasma (PRP) was obtained by centrifugation of human blood collected from healthy volunteers according to the RegenKit-BCT[®] procedures (RegenLab SA). An average of 4.5 mL of PRP containing 1.8×10^9 platelets were obtained from 8 mL of blood. Mouse PRP was obtained by centrifugation of blood collected from C57BL/6J^{su9-DsRed2} mice (Hasuwa et al., 2010; Dong et al., 2017). An average of 10^9 platelets were obtained per mL of blood, as previously reported (Jirouskova et al., 2007).

To inhibit mitochondrial respiration, platelets were treated for 3 h with 2 μ M rotenone (Sigma-Aldrich, Cat#R8875) and 2 μ M antimycin A (Sigma-Aldrich, Cat#A8674), inhibitors of complex I and complex III of the respiratory chain, respectively. Prior to be used, human untreated and ROT/AA-treated platelets were washed 3 times in serum-free DMEM containing heparine (20 U/mL) to avoid platelet aggregation.

Evaluation of mitochondria transfer from platelets to MSCs and assessment of endocytosis mechanisms

To assess transfer of mitochondria from human or mouse platelets to MSCs, MSCs were incubated with wheat germ agglutinin (WGA) conjugated to Alexa Fluor 647 (5 μ g/mL; Invitrogen, Cat#W32466) prior to their exposure for 24 h to either human platelets previously labelled with Mitotracker Green FM (40 nM, Invitrogen, Cat#M7514) or mouse platelets isolated from C57BL/6J^{su9-DsRed2} mice whose cells carry mitochondrially localized red fluorescent protein. The platelets were used at 8×10^7 /mL medium. The presence of human or mouse platelet-derived mitochondria in MSCs was detected by LSR Fortessa X20 flow cytometer (BD Biosciences) or LSM800 confocal microscopy (Zeiss).

To characterize the endocytosis process by which MSCs internalize platelet's mitochondria, human MSCs were co-cultivated with human platelets previously labelled with Mitotracker Green FM (40 nM, Invitrogen, Cat#M7514) in presence of macropinocytosis inhibitor 5-(N-Ethyl-N-Isopropyl)-amyloride, (50 μ M, Sigma-Aldrich, Cat#A3085), connexin 43 gap junction blocker Gap26, (300 μ M, MedChemexpress, Cat#HY-P1082), caveolae-mediated endocytosis inhibitors including β -cyclodextrin, (5mM, Santa Cruz Biotechnology, Cat#sc-204430), Genistein (200 μ M, Santa Cruz Biotechnology, Cat#sc-3515B) or Nystatin (50 μ M, Santa Cruz Biotechnology, Cat#sc-212431A) or dynamin dependent clathrin- mediated endocytosis inhibitor, Dynasore (50 μ M, Santa Cruz Biotechnology, Cat#sc-202592). After 24 h of treatment, the Mitotracker Green FM (40 nM, Invitrogen, Cat#M7514) fluorescence of MSCs was analysed by flow cytometry. Viability of MSCs following 24 hours of treatment with 50 μ M Dynasore was assessed by MTT assay. Briefly, cells were incubated with 3-(4,5-dimethylthiazol-2-yl)-2,5-diphenyltetrazolium bromide (MTT) (0.5mg/ml, Sigma-Aldrich, Cat#M2003) during 4 hours in a humidified atmosphere (e.g., +37°C, 5-6.5% CO₂). The ability of viable cells to reduce the soluble MTT into purple-colored formazan crystals was measured, after complete solubilization with DMSO, on a Tecan Infinite M200 Pro plate reader (Tecan) at the absorbance of 550nm.

Flow cytometry quantification of Mitofusin 2 protein expression

Protein expression Mitofusin-2 was quantified in MSCs after 24 h exposure to either intact platelets or ROT/AA-treated platelets cell fixation and permeabilization using Cytotfix/Cytoperm™ Fixation/Permeabilization kit (BD Pharmingen, Cat#554714) followed by intercellular staining with mouse monoclonal anti-Mitofusin 2 antibody (1 μ g/10⁶ cells, Abcam, Cat#ab56889) or mouse IgG2c Isotype Control Antibody (1 μ g/mL, Abcam, Cat#ab170191). Cells were then stained with a secondary goat anti mouse IgG antibody conjugated to Dylight 488 (1:500, Abcam, Cat#ab96871) prior to by analysed by flow cytometry.

Transmission Electron Microscopy

After coating 14 mm glass slides with 0.2% gelatin (Millipore, Cat#104078) in 12-well plates, MSCs were seeded at 10⁵ cells/mL and exposed to untreated or ROT/AA-treated platelets for 2, 4, 6 and 24 hours. The cells were then washed 3 times in 0.1 M PBS and fixed with 3% glutaraldehyde (Sigma-Aldrich, Cat#49629). Cells were washed again 3 times in 0.1 M PBS prior to be exposed to 1 % osmium tetroxide (Electron Microscopy Science, Cat#19190)

diluted in 0.1 M PBS for 1 h at 4 °C. After 3 washes with H₂O, cells were gradually dehydrated in graded series of chilled ethanol (70 %, 90 %, 100 % for 15 min each) (Carlo Erba, Cat#528131) at room temperature. Cells were gradually infiltrated with resin (Electron Microscopy Science, Cat#14120) at room temperature. Gelatin capsules (Electron Microscopy Science, Cat#70105) were put upside-down on the coverslips and polymerized 24 hours at 60 °C. Samples were lightly heated to remove glass coverslip and were cut on an ultramicrotome Reichert S (Leica Biosystems). Acquisitions were performed on a JEOL 1011 TEM with a Gatan Orius 1000 CCD Camera.

Flow cytometry analysis of cell proliferation and cell survival

To assess MSC proliferation in the presence of platelets, MSCs were stained with 0.2 μM carboxyfluorescein diacetate succinimidyl ester (CFSE; Invitrogen, Cat#C34554) prior to be exposed to various concentrations (2×10^7 , 4×10^7 or 8×10^7 /mL) of untreated or ROT/AA-treated platelets.

To induce oxidative stress and apoptosis, MSCs were exposed to 600 μM H₂O₂ in FBS-free DMEM for 2 h prior to be exposed to various concentrations of untreated or ROT/AA-treated platelets for 24 h. The cells were then stained with annexin V conjugated to phycoerythrin and with 7-aminoactinomycin D (7AAD; BD Pharmingen, Cat#559763) according to the manufacturer's instructions and analyzed by LSR Fortessa X20 flow cytometer. The number ratio of living MSCs was calculated as the percentage of the double negative stained cells relative to the total counted cells.

Collection of conditioned media

MSCs seeded at 10^5 cells/mL were exposed to various concentrations (2×10^7 , 4×10^7 or 8×10^7 /mL) of untreated or ROT/AA-treated platelets for 24 h. The supernatants were then collected, centrifuged at 4,300 rpm for 5 min to remove cell debris and platelets, and kept frozen until use.

ELISA assays

The secretion levels of VEGF and HGF by MSCs following their exposure to various concentrations (2×10^7 , 4×10^7 or 8×10^7 /mL) of human untreated or ROT/AA-treated platelets or following 24h exposure to mitochondria isolated from platelets were measured by enzyme-linked immunosorbent (ELISA) assays (PeproTech, Cat#BGK14210, Cat#900-K10, Cat#900-K00) according to the manufacturer's instructions. Absorbance measurements were carried out on a Tecan Infinite M200 Pro plate reader (Tecan) combined with the acquisition software

Magellan™ 7.2 (Tecan). Cytokine concentrations were calculated from the calibration curves obtained from serial dilutions of standard protein. Cytokine concentrations in conditioned media containing only platelets were also measured and subtracted to the cytokine concentrations obtained with conditioned media from MSCs following their exposure to platelets.

Real-time PCR assays

RNAs were extracted from mouse cutaneous wounds, mouse skeletal muscles or cultured MSCs by using the RNeasy Fibrous Tissue Mini Kit (Qiagen, Cat#74704), TRIzol™ Reagent (Invitrogen, Cat#15596026) or the NucleoSpin® RNA spin kit (MACHEREY-NAGEL GmbH & Co. KG, Cat#740955.250), respectively. Reverse transcription was performed using the SuperScript™ III Reverse Transcriptase kit (Invitrogen, Cat#18080044) and random primers. Quantitative RT-PCR (qPCR) reactions were performed in duplicates by using the PowerUp™ SYBR™ Green Master Mix (Applied Biosystems, Cat#A25742) and the StepOnePlus™ detection system (Applied Biosystems) associated with the acquisition and analysis StepOne™ software v2.1 (Applied Biosystems). PCR conditions were as follows: 10 minutes at 95°C followed by 40 cycles comprising one step at 95°C for 15 seconds and one step at 60°C for 1 minute and a final cycle of 15 seconds at 95°C, 1 minute at 60°C and 15 seconds at 95°C. The human or mouse TATA-Binding Protein (TBP) mRNAs were used as references for the quantification of human or mouse transcripts of interest, respectively. The sequences of the primers used in this study are listed in the Supplementary Table 1.

Immunocytochemistry

Following 24 hours exposure to human intact platelets or ROT/AA-treated platelets, MSCs were fixed with 4% PFA and stained with antibodies against FAS (1:100, rabbit monoclonal antibody, Abcam, Cat#ab99359, RRID: AB_10697253) or ACLY (1:50, rabbit monoclonal antibody, Abcam, Cat#ab40793, RRID: AB_722533). For ACC staining (1:100, rabbit monoclonal antibody, Abcam, Cat#ab109368, RRID: AB_10864809), MSCs were fixed with methanol. Samples were then exposed to Cy3- conjugated secondary goat anti-rabbit antibody (1:100, Abcam, Cat#ab6939, RRID: AB_955021). Nuclei were counterstained with Hoechst 33342 (Sigma-Aldrich, Cat#B2261). Fluorescence was analyzed with a Zeiss Axioplan 2 Imaging microscope.

Seahorse analysis

The bioenergetic profile of MSCs alone or after treatment with 8×10^7 platelets/mL medium was assessed using the Seahorse Bioscience XF24 Analyzer (Agilent) that provides real-time evaluation of the oxygen consumption rate (OCR), indicative of mitochondrial respiration, and extracellular acidification rate (ECAR), an index of glycolysis. Cells were seeded at the density of 2×10^4 cells/well and were exposed to untreated or ROT/AA-treated platelets for 24 h. The cells were washed several times with PBS to eliminate platelets. Seahorse measurements were performed in FCS- and bicarbonate-free DMEM (pH 7.4) supplemented with 5.5 mM glucose, 1% glutamax and 1% sodium pyruvate (Sigma-Aldrich, Cat#P2256). The bioenergetic profile of the cells was evaluated using the Agilent Seahorse XF Cell Mito Stress Test, with sequential additions of 1 $\mu\text{g/mL}$ oligomycin, an inhibitor of ATP synthase (Sigma-Aldrich, Cat#O4876), 0.7 $\mu\text{mol/L}$ of the uncoupling agent, carbonyl cyanide 4-(trifluoromethoxy) phenylhydrazone (FCCP, Sigma-Aldrich, Cat#C2910) and 1 $\mu\text{mol/L}$ rotenone and 1 $\mu\text{mol/L}$ antimycin A to inhibit complex I and complex III of the respiratory chain, respectively. Baseline cellular OCR was initially obtained, from which basal respiration was derived by subtracting non-mitochondrial respiration following addition of ROT/AA. ATP-linked respiration was calculated by subtracting the oligomycin rate from baseline cellular OCR. Proton leak respiration was calculated by subtracting non-mitochondrial respiration from the oligomycin rate. Maximal respiratory capacity was derived by subtracting non-mitochondrial respiration from the FCCP rate. Mitochondrial reserve capacity was calculated by subtracting basal respiration from maximal respiratory capacity. Coupling efficiency was determined by calculating the percentage of OCR immediately following the oligomycin treatment over the final baseline value. At the end of the assay, the cells in the wells were lysed with RIPA buffer (Thermo Scientific, Cat#89900) and protein quantifications were made using the Pierce™ protein assay kit (Thermo Scientific, Cat#23227) based on the bicinchoninic acid (BCA) method. Results were analyzed using Seahorse Wave Desktop Software (Agilent) and were normalized by protein content.

ATP assay and estimation of the adenylate energy charge

Intracellular ATP levels were evaluated using the ATPLite™ Bioluminescence Assay Kit (Perkin Elmer, Cat#6016943) according to the manufacturer's instructions.

The adenylate energy charge of MSCs was calculated using the following equation:

$$\frac{[ATP] + \frac{1}{2}[ADP]}{[ATP] + [ADP] + [AMP]} \text{ (Atkinson and Walton, 1967).}$$

Lactate dehydrogenase enzymatic activity

Intracellular lactate levels were evaluated using the L-Lactate assay kit (Abcam, Cat#ab65330) according to the manufacturer's instructions.

Citrate synthase enzymatic activity

MSCs were homogenized in ice-cold buffer (100 μ L per 2×10^5 cells) containing 5 mM HEPES sodium salt (Sigma-Aldrich, Cat#H7006), pH 8.7, 1 mM Ethylene glycol-bis(2-aminoethylether)-N,N,N',N'-tetraacetic acid (EGTA, Sigma-Aldrich, Cat#03777), 1 mM DL-Dithiothreitol (DTT, Sigma-Aldrich, Cat#D0632) and 0.1% Triton™ X-100 (Sigma-Aldrich, Cat#T9284). Total activity of citrate synthase (CS) was assessed at 30 °C, adjusted at pH 7.5 with potassium hydroxide (Sigma-Aldrich, Cat#P5958) using a standard spectrophotometric assays (Caffin et al., 2013). Briefly, CS activity was monitored in a 100 mM Tris buffer (Trizma® base, Sigma-Aldrich, Cat#T1503) in the presence of Acetyl-CoA (300 μ M, Acetyl coenzyme A lithium salt, Sigma-Aldrich, Cat#A2181). The reaction was initiated by the addition of oxaloacetic acid (500 μ M, Sigma-Aldrich Cat#O4126) and the production of Coenzyme A (CoASH) from CS was followed by measuring the production of mercaptic ions at 412 nm in the presence of 5,5-Dithiobi-2-nitrobenzoic acid (DTNB, 100 μ M, Sigma-Aldrich, Cat#D8130).

Preparation of MSCs for metabolomic analysis

Sample preparations for metabolomic analysis was conducted as previously described (Izzo et al., 2017). Briefly, 10^5 MSCs were seeded on 6-well plates and incubated for 24 h in the absence or presence of 8×10^7 platelets/mL medium. For each condition, 2×10^5 MSCs were removed at the end of the incubation and placed in 1 mL of cold methanol (Sigma-Aldrich, Cat#646377) / water (9:1). Three hundred microliters of the extracted methanol solution were dried, incubated overnight with 20mg/ml of pyridine (Sigma-Aldrich, Cat#270407) in methoxyamine hydrochloride (Sigma-Aldrich, Cat#226904), then incubated for 30 min at 37°C with 1% N-Methyl-N-(trimethylsilyl)trifluoroacetamide (Sigma-Aldrich, Cat#69479) in chlorotrimethylsilane (Sigma-Aldrich, Cat#95541) and used for gas chromatography-mass spectrometry (GC-MS) assay. Three hundred microliters of methanol extracts were dried, resuspended in water and used for liquid chromatography-mass spectrometry evaluation (LC-MS) (Izzo et al., 2017).

Analysis of intracellular metabolites by gas chromatography and ultra-high performance liquid chromatography coupled to mass spectrometry

Analysis of intracellular metabolites was performed as previously described (Izzo et al., 2017). The GC-MS/MS method was performed using a 7890B gas chromatography (Agilent Technologies) coupled to a triple quadrupole 7000C mass spectrometer (Agilent Technologies) equipped with a high-sensitivity electronic impact source (EI) operating in the positive mode. The ultra-high performance liquid chromatography (UHPLC)-MS/MS assay was performed using the RRLC 1260 system (Agilent Technologies) coupled to a Triple Quadrupole 6410 mass spectrometer (Agilent Technologies) equipped with an electrospray source operating in the positive mode. Peak detection and integration of the analytes were performed using the Agilent MassHunter quantitative software (B.07.01).

Metabolomics data analysis

To further characterize the metabolic changes and the metabolic pathways involved, individual metabolites were processed and analyzed using MetaboAnalyst 4.0 (www.metaboanalyst.ca) (Chong et al., 2018, RRID: SCR_015539). Two modules of MetaboAnalyst were used, i.e. the pathway analysis and the enrichment analysis, which are based on the KEGG PATHWAY Database (Bioinformatics Center & Human Genome Center, www.genome.jp/kegg/pathway.html) and Small Molecule Pathway Database (The Metabolomics Innovation Centre, smpdb.ca), respectively (Frolkis et al., 2010).

Mitochondria isolation and quantification

Mitochondria were isolated from human platelets using the Mitochondria Isolation Kit (Thermo Scientific, Cat#89874) according to the manufacturer's instructions. To reduce the contamination of mitochondrial preparation with other cytosolic structures, the samples were spun at 3000 g for 15 minutes. The concentration of mitochondrial proteins was measured using the Pierce™ protein assay kit (Thermo Scientific, Cat#23227) based on the bicinchoninic acid (BCA) method. The equivalent of 0.5µg of mitochondrial proteins was used to treat $2 \cdot 10^5$ MSCs for 24 hours prior to be grafted into mouse Tibialis Anterior.

Cell injection into mouse tibialis anterior muscles

All animal experiments were performed according to National and European community guidelines, and protocols were approved by French Ministry of research and higher education (project approval numbers # A94028379) after ethical committee agreement. 2 month-old male α -sarcoglycan deficient ($sgca^{nul}$) mice were used as animal model for autosomal recessive muscular dystrophy. $Sgca^{nul}$ mice were anesthetized with isoflurane prior to the delivery of $2 \cdot 10^5$ of untreated MSCs, MSCs in combination with 8×10^6 human platelets or

MSC pretreated with isolated mitochondria in the Tibialis Anterior (TA) muscles. Cells were resuspended in a final volume of 20 μ l of Hank's. TA were injected with 20 μ l of HBSS. Mice were sacrificed by cervical dislocation 3 or 7 days following the graft. TA muscles were dissected as described previously (Shinin et al., 2009). Briefly, the skin of the lower limbs was removed exposing the muscles below the knee. The connective tissue around the TA was gently released and the tendon of the TA was excised at the most distal part of the muscle. The muscle is then lifted from the leg and cut at the tendon at the knee bone. The isolated muscles were frozen rapidly in liquid nitrogen for RNA extraction, and stored at -80°C.

Mouse cutaneous wounds and cell grafting

All experiments were performed according to the institutional guidelines for animal care and were approved by the local ethics committee COMETH (project approval numbers # 20-025 and # 10/11/15-7B) and the French Ministry of Agriculture (project approval numbers # B94028245 and # A-05194.02). Full thickness cutaneous wounds were created on the back of 8-week-old male mice C57BL/6JRj (Janvier Laboratories, Cat#2670020, RRID: MGI:2670020), according to the Galiano's murine healing model (Galiano et al., 2004). This model minimizes rodent wound contractions and therefore mimics wound healing processes occurring in humans including granulation tissue formation and re-epithelialization. Briefly, animals were anesthetized by isoflurane, initiation at 3.5 and maintenance at 1.5. The dorsal surface was shaved with an electric clipper and sterilized with 70 % alcohol. Four circular, full thickness 5 mm diameter cutaneous wounds were created on the back of each mouse (2 wounds on each side of the midline) by using a sterile 5-mm biopsy punch (Kai Medical, Cat#BP-50F) (Supplementary Figure 6A). Sterile donut-shaped silicone splints were fixed to the surrounding wound edge with an adhesive film (3M™ Vetbond™ Tissue Adhesive, Cat#1469SB) and interrupted 6-0 silk thread sutures (ETHILON® Nylon Suture, Cat#697G) to prevent skin retraction (Supplementary Figure 6B). Immediately after the skin injuries, each wound was injected with 100 μ L of Hank's Balanced Salt Solution (HBSS) containing either 2×10^5 MSCs alone or in combination with untreated or ROT/AA-treated platelets activated with 10 % CaCl₂. Control wounds were injected with either saline solution (HBSS) or CaCl₂-activated untreated or ROT/AA-treated platelets alone. Platelets were used at 8×10^7 /mL medium. In some experiments, MSCs were delivered in the presence of 10 mM sodium citrate tribasic dihydrate (Sigma-Aldrich, Cat#S4641). A non-adherent clear wound dressing (Telfa™, Covidien, Cat#1109) was then placed to cover the wounds and maintained with adherent dressing (3M™ Tegaderm™ Transparent Film Dressing, Cat#1620). The

animals were placed in recovery cages under a warming lamp and allowed fully recover from anesthesia before returning to their cages in the animal facilities. Pain was monitored by pre-medication 30 min before skin injury and every 12h during 3 days with i.p. injection of buprenorphine at 0,1mg/kg.

Wound closure analysis

Digital photographs were taken on the day of surgery and 3 and 7 days thereafter (Supplementary Figure 6C). The removal of the non-adherent clear wound dressing was done the 3rd day after the wound creation to allow photographs. Photographs were taken with a millimetric ruler that was used to normalize the wound sizes (Supplementary Figure 6C and D). Wound closure was quantified using ImageJ software (1.52, National Institutes of Health (NIH)) in a blinded manner by means of evaluation of the wound re-epithelialization on days 3 and 7 post-surgery and was calculated as follows: $[1 - (\text{wound area on day X}) / \text{wound area on day 0}] \times 100$ (Supplementary Figure 6D). The mice were euthanized at day 3 or day 7 from the time of wounding. The wounds were excised, dissected, and immediately frozen for molecular biology analyses.

Immunohistochemical evaluation of angiogenesis in mouse wounds

Immunohistochemical measurements of angiogenesis were performed at day-3 and day-7 post-surgery. After animal sacrifice, mouse wounds were harvested, fixed in 4% neutral buffered formalin for 48 h, dehydrated with a gradient alcohol series, cleared in xylene and embedded in paraffin. Tissue sections (5 μm) were deparaffinized, hydrated and pretreated for antigen retrieval with citrate buffer. Sections were then incubated with a rat anti-mouse CD31 antibody (1:400, BD Pharmingen, Cat#550274, RRID: AB_393571) followed by exposure to Alexa Fluor 555 goat anti-rat IgG (1:500, Invitrogen, Cat#A-21434, RRID: AB_2535855). Nuclei were stained with Hoechst 33342 (Sigma-Aldrich, Cat#B2261). Fluorescence was analyzed by conventional Zeiss Axioplan 2 Imaging microscopy.

Capillary density of healing area was determined by counting CD31-stained endothelial cells from at least 10 randomly selected fields/wound.

MSCs implantation procedure for bone formation

Three male of 7 weeks-old SCID mice were used (Charles River Laboratories). The experimental protocol was approved by the local ethical committee (Anses/ENVA/UPEC n°18/11/14-1). Isoflurane was used for anaesthesia. 6 subcutaneous dorsal pockets (0.5 cm

incisions) were prepared per mouse. In 4 pockets, bone chips-TPB (Tutoplast[®]-processed bone, Tutogen Medical, EFS-Ile de France) granules sizing 2–3 mm and weighing 8.0 ± 1 mg were placed (and 2 stay empty) then 20 μ l containing 3.10^5 hMSCs associated to human platelets were injected in 2 pockets containing bone chips-TPB and in the 2 pockets without bone chips. The skin was closed by suture with 5–0 sutures (Technicon, Help Medical, Cat#ETF2831). The 2 pockets containing bone chips alone served as a negative control. These experiments were performed in sixplicate in three independent animals ($n= 6$ per group). After 7 weeks, animals were euthanized by over-dose of pentobarbital. The skin was opened from the vertebral column, pictures were taken and the specimens were excised and immediately fixed in ethanol 70%.

MSC-mediated bone formation histology

Specimens were decalcified 3 h in 6.8% nitric acid (VWR, Cat#20413.241) then rinsed in tap water before being embedded in paraffin. Sections of 3 μ m were made using a microtome (Microm HM355S, ThermoFisher Scientific) and stained with Masson's trichrome. The images were acquired with a standard light microscope (Olympus, CX41) using a Digital Color Camera (UC30) and CellSens Entry software (Olympus). Fifteen sections of each sample were analyzed (5 at the beginning, 5 in the middle and 5 at the end of the bone particle scaffold).

QUANTIFICATION AND STATISTICAL ANALYSIS

Data analysis was performed using GraphPad Prism software version 6.0 (San Diego, CA). Data are expressed as mean \pm SD. For statistical analysis of data obtained from $n \geq 5$ independent experiments, parametric tests were used after validation of normality and equality of variances of populations by using Shapiro-Wilk and Browne-Forsythe tests, respectively. Otherwise, non-parametric tests including one-way ANOVA on rank followed by Dunn's multiple comparisons were used. For statistical analysis of data obtained from $n < 5$ experiments, non-parametric tests were applied. In particular, metabolomics data were analysed using a one-way ANOVA on rank followed by Conover-Iman pairwise comparisons and the P -values were adjusted with Benjamini-Hochberg method to control the False-Discovery Rate (FDR) (Alonso, Marsal et Julià, 2015; Zhu et al., 2019). For the other small sample size experiments, data were analysed by one-way ANOVA on rank followed by Dunn's multiple comparisons. All P values and n are reported in the figure legends. Results are considered significant when $P < 0.05$. The statistical method used for each experiment is

indicated in each figure legend. For *in vivo* studies, mice were randomly assigned to the different wound treatment groups. Investigator were blinded to wound treatment allocation during the experiments as well as during the analysis. No statistical method was used to predetermine sample size.

ADDITIONAL RESOURCES

REFERENCES

- Acquistapace, A., Bru, T., Lesault, P.-F., Figeac, F., Coudert, A.E., le Coz, O., Christov, C., Baudin, X., Auber, F., Yiou, R., et al. (2011). Human mesenchymal stem cells reprogram adult cardiomyocytes toward a progenitor-like state through partial cell fusion and mitochondria transfer. *Stem Cells Dayt. Ohio* 29, 812–824.
- Al Amir Dache, Z., Otandault, A., Tanos, R., Pastor, B., Meddeb, R., Sanchez, C., Arena, G., Lasorsa, L., Bennett, A., Grange, T., et al. (2020). Blood contains circulating cell-free respiratory competent mitochondria. *FASEB J. Off. Publ. Fed. Am. Soc. Exp. Biol.*
- Alonso, A., Marsal, S., and Julià, A. (2015). Analytical methods in untargeted metabolomics: state of the art in 2015. *Front. Bioeng. Biotechnol.* 3, 23.
- Andia, I., Martin, J.I., and Maffulli, N. (2018). Platelet-rich Plasma and Mesenchymal Stem Cells: Exciting, But ... are we there Yet? *Sports Med. Arthrosc. Rev.* 26, 59–63.
- Atkinson, D.E., and Walton, G.M. (1967). Adenosine triphosphate conservation in metabolic regulation. Rat liver citrate cleavage enzyme. *J. Biol. Chem.* 242, 3239–3241.
- Bahat, A., and Gross, A. (2019). Mitochondrial plasticity in cell fate regulation. *J. Biol. Chem.* 294, 13852–13863.
- Berg, J.M., Tymoczko, J.L., and Stryer, L. (2002). Entry to the Citric Acid Cycle and Metabolism Through It Are Controlled. *Biochem.* 5th Ed.
- Berridge, M.V., McConnell, M.J., Grasso, C., Bajzikova, M., Kovarova, J., and Neuzil, J. (2016). Horizontal transfer of mitochondria between mammalian cells: beyond co-culture approaches. *Curr. Opin. Genet. Dev.* 38, 75–82.
- Binu, S., Soumya, S.J., and Sudhakaran, P.R. (2013). Metabolite control of angiogenesis: angiogenic effect of citrate. *J. Physiol. Biochem.* 69, 383–395.
- Boudreau, L.H., Duchez, A.-C., Cloutier, N., Soulet, D., Martin, N., Bollinger, J., Paré, A., Rousseau, M., Naika, G.S., Lévesque, T., et al. (2014). Platelets release mitochondria serving as substrate for bactericidal group IIA-secreted phospholipase A2 to promote inflammation. *Blood* 124, 2173–2183.

Bruning, U., Morales-Rodriguez, F., Kalucka, J., Goveia, J., Taverna, F., Queiroz, K.C.S., Dubois, C., Cantelmo, A.R., Chen, R., Lorocho, S., et al. (2018). Impairment of Angiogenesis by Fatty Acid Synthase Inhibition Involves mTOR Malonylation. *Cell Metab.* *28*, 866-880.e15.

Caicedo, A., Fritz, V., Brondello, J.-M., Ayala, M., Dennemont, I., Abdellaoui, N., de Fraipont, F., Moisan, A., Prouteau, C.A., Boukhaddaoui, H., et al. (2015). MitoCeption as a new tool to assess the effects of mesenchymal stem/stromal cell mitochondria on cancer cell metabolism and function. *Sci. Rep.* *5*, 9073.

Chen, J., Zhang, Z.G., Li, Y., Wang, L., Xu, Y.X., Gautam, S.C., Lu, M., Zhu, Z., and Chopp, M. (2003). Intravenous administration of human bone marrow stromal cells induces angiogenesis in the ischemic boundary zone after stroke in rats. *Circ. Res.* *92*, 692–699.

Chevallier, N., Anagnostou, F., Zilber, S., Bodivit, G., Maurin, S., Barrault, A., Bierling, P., Hernigou, P., Layrolle, P., and Rouard, H. (2010). Osteoblastic differentiation of human mesenchymal stem cells with platelet lysate. *Biomaterials* *31*, 270–278.

Chicharro-Alcántara, D., Rubio-Zaragoza, M., Damiá-Giménez, E., Carrillo-Poveda, J.M., Cuervo-Serrato, B., Peláez-Gorrea, P., and Sopena-Juncosa, J.J. (2018). Platelet Rich Plasma: New Insights for Cutaneous Wound Healing Management. *J. Funct. Biomater.* *9*.

De la Fuente, I.M., Cortés, J.M., Valero, E., Desroches, M., Rodrigues, S., Malaina, I., and Martínez, L. (2014). On the dynamics of the adenylate energy system: homeorhesis vs homeostasis. *PLoS One* *9*, e108676.

De Pascale, M.R., Sommese, L., Casamassimi, A., and Napoli, C. (2015). Platelet derivatives in regenerative medicine: an update. *Transfus. Med. Rev.* *29*, 52–61.

D'Ippolito, G., Diabira, S., Howard, G.A., Menei, P., Roos, B.A., and Schiller, P.C. (2004). Marrow-isolated adult multilineage inducible (MIAMI) cells, a unique population of postnatal young and old human cells with extensive expansion and differentiation potential. *J. Cell Sci.* *117*, 2971–2981.

Dong, L.-F., Kovarova, J., Bajzikova, M., Bezawork-Geleta, A., Svec, D., Endaya, B., Sachaphibulkij, K., Coelho, A.R., Sebkova, N., Ruzickova, A., et al. (2017). Horizontal transfer of whole mitochondria restores tumorigenic potential in mitochondrial DNA-deficient cancer cells. *ELife* *6*.

Duan, J., Chen, L., Zhou, M., Zhang, J., Sun, L., Huang, N., Bin, J., Liao, Y., and Liao, W. (2017). MACC1 decreases the chemosensitivity of gastric cancer cells to oxaliplatin by regulating FASN expression. *Oncol. Rep.* *37*, 2583–2592.

Etulain, J. (2018). Platelets in wound healing and regenerative medicine. *Platelets* *29*, 556–568.

Figeac, F., Lesault, P.-F., Le Coz, O., Damy, T., Souktani, R., Trébeau, C., Schmitt, A., Ribot, J., Mounier, R., Guguin, A., et al. (2014). Nanotubular crosstalk with distressed cardiomyocytes stimulates the paracrine repair function of mesenchymal stem cells. *Stem Cells Dayt. Ohio* *32*, 216–230.

Frezza, C. (2017). Mitochondrial metabolites: undercover signalling molecules. *Interface Focus* *7*, 20160100.

Gandia, C., Armiñan, A., García-Verdugo, J.M., Lledó, E., Ruiz, A., Miñana, M.D., Sanchez-Torrijos, J., Payá, R., Mirabet, V., Carbonell-Uberos, F., et al. (2008). Human dental pulp stem cells improve left ventricular function, induce angiogenesis, and reduce infarct size in rats with acute myocardial infarction. *Stem Cells Dayt. Ohio* *26*, 638–645.

Golchin, A., Farahany, T.Z., Khojasteh, A., Soleimanifar, F., and Ardehshirylajimi, A. (2019). The Clinical Trials of Mesenchymal Stem Cell Therapy in Skin Diseases: An Update and Concise Review. *Curr. Stem Cell Res. Ther.* *14*, 22–33.

Gremmel, T., Frelinger, A.L., and Michelson, A.D. (2016). Platelet Physiology. *Semin. Thromb. Hemost.* *42*, 191–204.

Henrichs, V., Grycova, L., Barinka, C., Nahacka, Z., Neuzil, J., Diez, S., Rohlena, J., Braun, M., and Lansky, Z. (2020). Mitochondria-adaptor TRAK1 promotes kinesin-1 driven transport in crowded environments. *Nat. Commun.* *11*, 3123.

Henschler, R., Gabriel, C., Schallmoser, K., Burnouf, T., and Koh, M.B.C. (2019). Human platelet lysate current standards and future developments. *Transfusion (Paris)* *59*, 1407–1413.

Hersant, B., Sid-Ahmed, M., Braud, L., Jourdan, M., Baba-Amer, Y., Meningaud, J.-P., and Rodriguez, A.-M. (2019). Platelet-Rich Plasma Improves the Wound Healing Potential of Mesenchymal Stem Cells through Paracrine and Metabolism Alterations. *Stem Cells Int.* *2019*, 1234263.

Holinstat, M. (2017). Normal platelet function. *Cancer Metastasis Rev.* *36*, 195–198.

Hull, F.E., and Whereat, A.F. (1967). The effect of rotenone on the regulation of fatty acid synthesis in heart mitochondria. *J. Biol. Chem.* *242*, 4023–4028.

Islam, M.N., Das, S.R., Emin, M.T., Wei, M., Sun, L., Westphalen, K., Rowlands, D.J., Quadri, S.K., Bhattacharya, S., and Bhattacharya, J. (2012a). Mitochondrial transfer from bone-marrow-derived stromal cells to pulmonary alveoli protects against acute lung injury. *Nat. Med.* *18*, 759–765.

Islam, M.N., Das, S.R., Emin, M.T., Wei, M., Sun, L., Westphalen, K., Rowlands, D.J., Quadri, S.K., Bhattacharya, S., and Bhattacharya, J. (2012b). Mitochondrial transfer from bone-marrow-derived stromal cells to pulmonary alveoli protects against acute lung injury. *Nat. Med.* *18*, 759–765.

Kawase, T. (2015). Platelet-rich plasma and its derivatives as promising bioactive materials for regenerative medicine: basic principles and concepts underlying recent advances. *Odontology* *103*, 126–135.

Kitani, T., Kami, D., Matoba, S., and Gojo, S. (2014). Internalization of isolated functional mitochondria: involvement of macropinocytosis. *J. Cell. Mol. Med.* *18*, 1694–1703.

Koyanagi, M., Brandes, R.P., Haendeler, J., Zeiher, A.M., and Dimmeler, S. (2005). Cell-to-cell connection of endothelial progenitor cells with cardiac myocytes by nanotubes: a novel mechanism for cell fate changes? *Circ. Res.* *96*, 1039–1041.

Leotot, J., Coquelin, L., Bodivit, G., Bierling, P., Hernigou, P., Rouard, H., and Chevallier, N. (2013). Platelet lysate coating on scaffolds directly and indirectly enhances cell migration, improving bone and blood vessel formation. *Acta Biomater.* *9*, 6630–6640.

Li, H., Wang, C., He, T., Zhao, T., Chen, Y., Shen, Y., Zhang, X., and Wang, L. (2019). Mitochondrial Transfer from Bone Marrow Mesenchymal Stem Cells to Motor Neurons in Spinal Cord Injury Rats via Gap Junction. *Theranostics* *9*, 2017–2035.

Li, L., Chen, X., Wang, W.E., and Zeng, C. (2016). How to Improve the Survival of Transplanted Mesenchymal Stem Cell in Ischemic Heart? *Stem Cells Int.* *2016*, 9682757.

- Lindholm, C., and Searle, R. (2016). Wound management for the 21st century: combining effectiveness and efficiency. *Int. Wound J.* *13 Suppl 2*, 5–15.
- Liu, K., Ji, K., Guo, L., Wu, W., Lu, H., Shan, P., and Yan, C. (2014). Mesenchymal stem cells rescue injured endothelial cells in an in vitro ischemia-reperfusion model via tunneling nanotube like structure-mediated mitochondrial transfer. *Microvasc. Res.* *92*, 10–18.
- Mahmoudian-Sani, M.-R., Rafeei, F., Amini, R., and Saidijam, M. (2018). The effect of mesenchymal stem cells combined with platelet-rich plasma on skin wound healing. *J. Cosmet. Dermatol.* *17*, 650–659.
- Mahrouf-Yorgov, M., Augeul, L., Da Silva, C.C., Jourdan, M., Rigolet, M., Manin, S., Ferrera, R., Ovize, M., Henry, A., Guguin, A., et al. (2017). Mesenchymal stem cells sense mitochondria released from damaged cells as danger signals to activate their rescue properties. *Cell Death Differ.* *24*, 1224–1238.
- Marcoux, G., Duchez, A.-C., Rousseau, M., Lévesque, T., Boudreau, L.H., Thibault, L., and Boilard, E. (2017). Microparticle and mitochondrial release during extended storage of different types of platelet concentrates. *Platelets* *28*, 272–280.
- Martínez-Reyes, I., and Chandel, N.S. (2020). Mitochondrial TCA cycle metabolites control physiology and disease. *Nat. Commun.* *11*, 102.
- Marx, R.E. (2004). Platelet-rich plasma: evidence to support its use. *J. Oral Maxillofac. Surg. Off. J. Am. Assoc. Oral Maxillofac. Surg.* *62*, 489–496.
- McDonnell, E., Crown, S.B., Fox, D.B., Kitir, B., Ilkayeva, O.R., Olsen, C.A., Grimsrud, P.A., and Hirschey, M.D. (2016). Lipids Reprogram Metabolism to Become a Major Carbon Source for Histone Acetylation. *Cell Rep.* *17*, 1463–1472.
- Melchinger, H., Jain, K., Tyagi, T., and Hwa, J. (2019). Role of Platelet Mitochondria: Life in a Nucleus-Free Zone. *Front. Cardiovasc. Med.* *6*, 153.
- Menendez, J.A., and Lupu, R. (2017). Fatty acid synthase regulates estrogen receptor- α signaling in breast cancer cells. *Oncogenesis* *6*, e299.
- Nakhle, J., Rodriguez, A.-M., and Vignais, M.-L. (2020). Multifaceted Roles of Mitochondrial Components and Metabolites in Metabolic Diseases and Cancer. *Int. J. Mol. Sci.* *21*, 4405.
- Patel, D., Rorbach, J., Downes, K., Szukszto, M.J., Pekalski, M.L., and Minczuk, M. (2017). Macropinocytic entry of isolated mitochondria in epidermal growth factor-activated human osteosarcoma cells. *Sci. Rep.* *7*, 12886.
- Peiris-Pagès, M., Martinez-Outschoorn, U.E., Pestell, R.G., Sotgia, F., and Lisanti, M.P. (2016). Cancer stem cell metabolism. *Breast Cancer Res. BCR* *18*, 55.
- Pope, E.D., Kimbrough, E.O., Vemireddy, L.P., Surapaneni, P.K., Copland, J.A., and Mody, K. (2019). Aberrant lipid metabolism as a therapeutic target in liver cancer. *Expert Opin. Ther. Targets* *23*, 473–483.
- Porporato, P.E., Filigheddu, N., Pedro, J.M.B.-S., Kroemer, G., and Galluzzi, L. (2018). Mitochondrial metabolism and cancer. *Cell Res.* *28*, 265–280.

- Qian, Y., Han, Q., Chen, W., Song, J., Zhao, X., Ouyang, Y., Yuan, W., and Fan, C. (2017). Platelet-Rich Plasma Derived Growth Factors Contribute to Stem Cell Differentiation in Musculoskeletal Regeneration. *Front. Chem.* *5*, 89.
- Rehman, J., Traktuev, D., Li, J., Merfeld-Clauss, S., Temm-Grove, C.J., Bovenkerk, J.E., Pell, C.L., Johnstone, B.H., Considine, R.V., and March, K.L. (2004). Secretion of angiogenic and antiapoptotic factors by human adipose stromal cells. *Circulation* *109*, 1292–1298.
- Rodriguez, A.-M., Pisani, D., Dechesne, C.A., Turc-Carel, C., Kurzenne, J.-Y., Wdziekonski, B., Villageois, A., Bagnis, C., Breittmayer, J.-P., Groux, H., et al. (2005a). Transplantation of a multipotent cell population from human adipose tissue induces dystrophin expression in the immunocompetent mdx mouse. *J. Exp. Med.* *201*, 1397–1405.
- Rodriguez, A.-M., Pisani, D., Dechesne, C.A., Turc-Carel, C., Kurzenne, J.-Y., Wdziekonski, B., Villageois, A., Bagnis, C., Breittmayer, J.-P., Groux, H., et al. (2005b). Transplantation of a multipotent cell population from human adipose tissue induces dystrophin expression in the immunocompetent mdx mouse. *J. Exp. Med.* *201*, 1397–1405.
- Rodriguez, A.-M., Nakhle, J., Griessinger, E., and Vignais, M.-L. (2018). Intercellular mitochondria trafficking highlighting the dual role of mesenchymal stem cells as both sensors and rescuers of tissue injury. *Cell Cycle* 1–25.
- Röhrig, F., and Schulze, A. (2016). The multifaceted roles of fatty acid synthesis in cancer. *Nat. Rev. Cancer* *16*, 732–749.
- Rowart, P., Erpicum, P., Detry, O., Weekers, L., Grégoire, C., Lechanteur, C., Briquet, A., Beguin, Y., Krzesinski, J.-M., and Jouret, F. (2015). Mesenchymal Stromal Cell Therapy in Ischemia/Reperfusion Injury. *J. Immunol. Res.* *2015*, 602597.
- Ryall, J.G. (2017). Simultaneous Measurement of Mitochondrial and Glycolytic Activity in Quiescent Muscle Stem Cells. *Methods Mol. Biol. Clifton NJ* *1556*, 245–253.
- Shen, L.C., Fall, L., Walton, G.M., and Atkinson, D.E. (1968). Interaction between energy charge and metabolite modulation in the regulation of enzymes of amphibolic sequences. Phosphofructokinase and pyruvate dehydrogenase. *Biochemistry* *7*, 4041–4045.
- Shi, Y., Shi, H., Nomi, A., Lei-Lei, Z., Zhang, B., and Qian, H. (2019). Mesenchymal stem cell-derived extracellular vesicles: a new impetus of promoting angiogenesis in tissue regeneration. *Cytotherapy* *21*, 497–508.
- Shinin, V., Gayraud-Morel, B., and Tajbakhsh, S. (2009). Template DNA-strand co-segregation and asymmetric cell division in skeletal muscle stem cells. *Methods Mol. Biol. Clifton NJ* *482*, 295–317.
- Spinelli, J.B., and Haigis, M.C. (2018). The multifaceted contributions of mitochondria to cellular metabolism. *Nat. Cell Biol.* *20*, 745–754.
- Tan, A.S., Baty, J.W., Dong, L.-F., Bezawork-Geleta, A., Endaya, B., Goodwin, J., Bajzikova, M., Kovarova, J., Peterka, M., Yan, B., et al. (2015). Mitochondrial genome acquisition restores respiratory function and tumorigenic potential of cancer cells without mitochondrial DNA. *Cell Metab.* *21*, 81–94.

Tobita, M., Tajima, S., and Mizuno, H. (2015). Adipose tissue-derived mesenchymal stem cells and platelet-rich plasma: stem cell transplantation methods that enhance stemness. *Stem Cell Res. Ther.* *6*, 215.

Wanet, A., Arnould, T., Najimi, M., and Renard, P. (2015). Connecting Mitochondria, Metabolism, and Stem Cell Fate. *Stem Cells Dev.* *24*, 1957–1971.

Wang, L., Zhang, T., Wang, L., Cai, Y., Zhong, X., He, X., Hu, L., Tian, S., Wu, M., Hui, L., et al. (2017). Fatty acid synthesis is critical for stem cell pluripotency via promoting mitochondrial fission. *EMBO J.* *36*, 1330–1347.

Williams, N.C., and O'Neill, L.A.J. (2018). A Role for the Krebs Cycle Intermediate Citrate in Metabolic Reprogramming in Innate Immunity and Inflammation. *Front. Immunol.* *9*, 141.

Yong, K.W., Choi, J.R., Mohammadi, M., Mitha, A.P., Sanati-Nezhad, A., and Sen, A. (2018). Mesenchymal Stem Cell Therapy for Ischemic Tissues. *Stem Cells Int.* *2018*, 8179075.

Zhao, Y., Jiang, Z., Delgado, E., Li, H., Zhou, H., Hu, W., Perez-Basterrechea, M., Janostakova, A., Tan, Q., Wang, J., et al. (2017). Platelet-Derived Mitochondria Display Embryonic Stem Cell Markers and Improve Pancreatic Islet β -cell Function in Humans. *Stem Cells Transl. Med.* *6*, 1684–1697.

Zhou, Y., Jin, G., Mi, R., Zhang, J., Zhang, J., Xu, H., Cheng, S., Zhang, Y., Song, W., and Liu, F. (2016). Inhibition of fatty acid synthase suppresses neovascularization via regulating the expression of VEGF-A in glioma. *J. Cancer Res. Clin. Oncol.* *142*, 2447–2459.

Zhu, A., Srivastava, A., Ibrahim, J.G., Patro, R., and Love, M.I. (2019). Nonparametric expression analysis using inferential replicate counts. *Nucleic Acids Res.* *47*, e105.

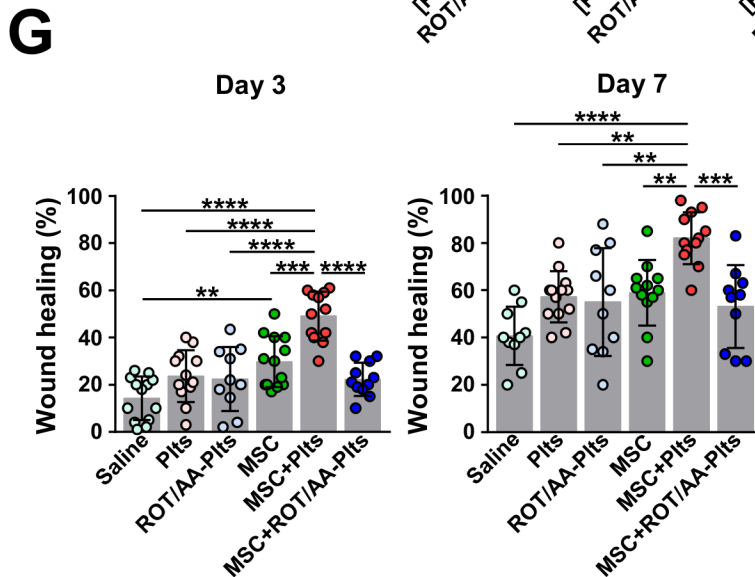
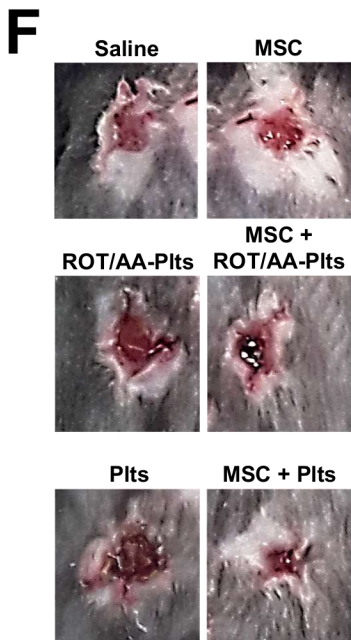
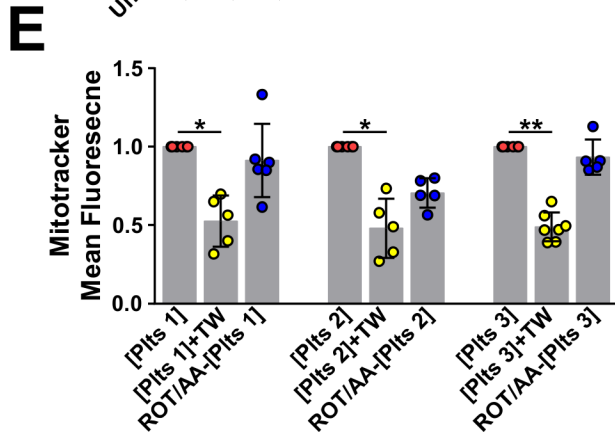
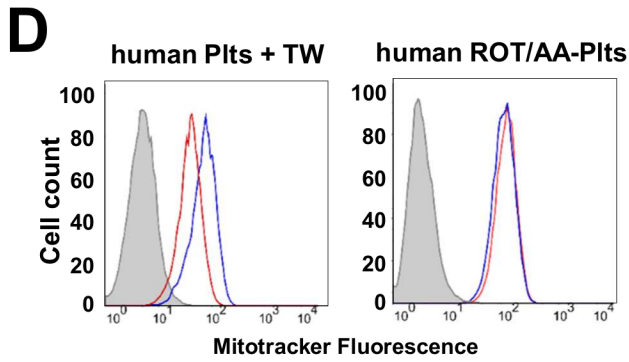
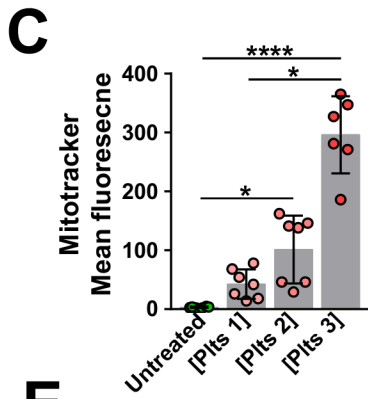
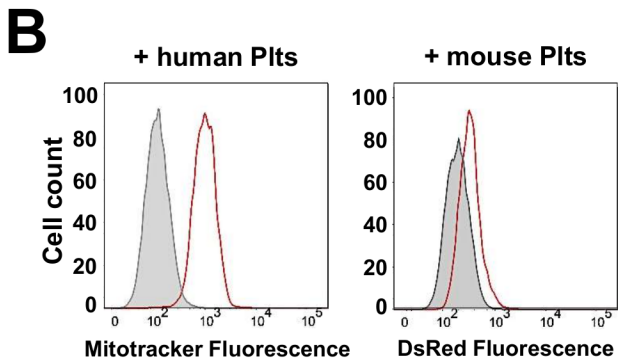
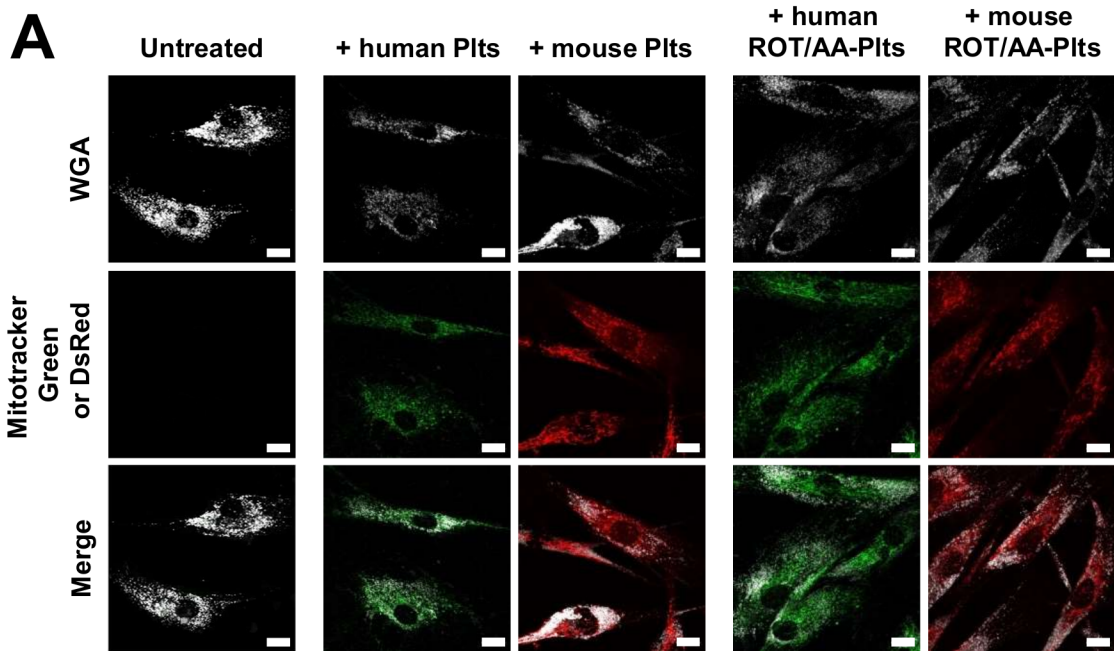


Figure 1

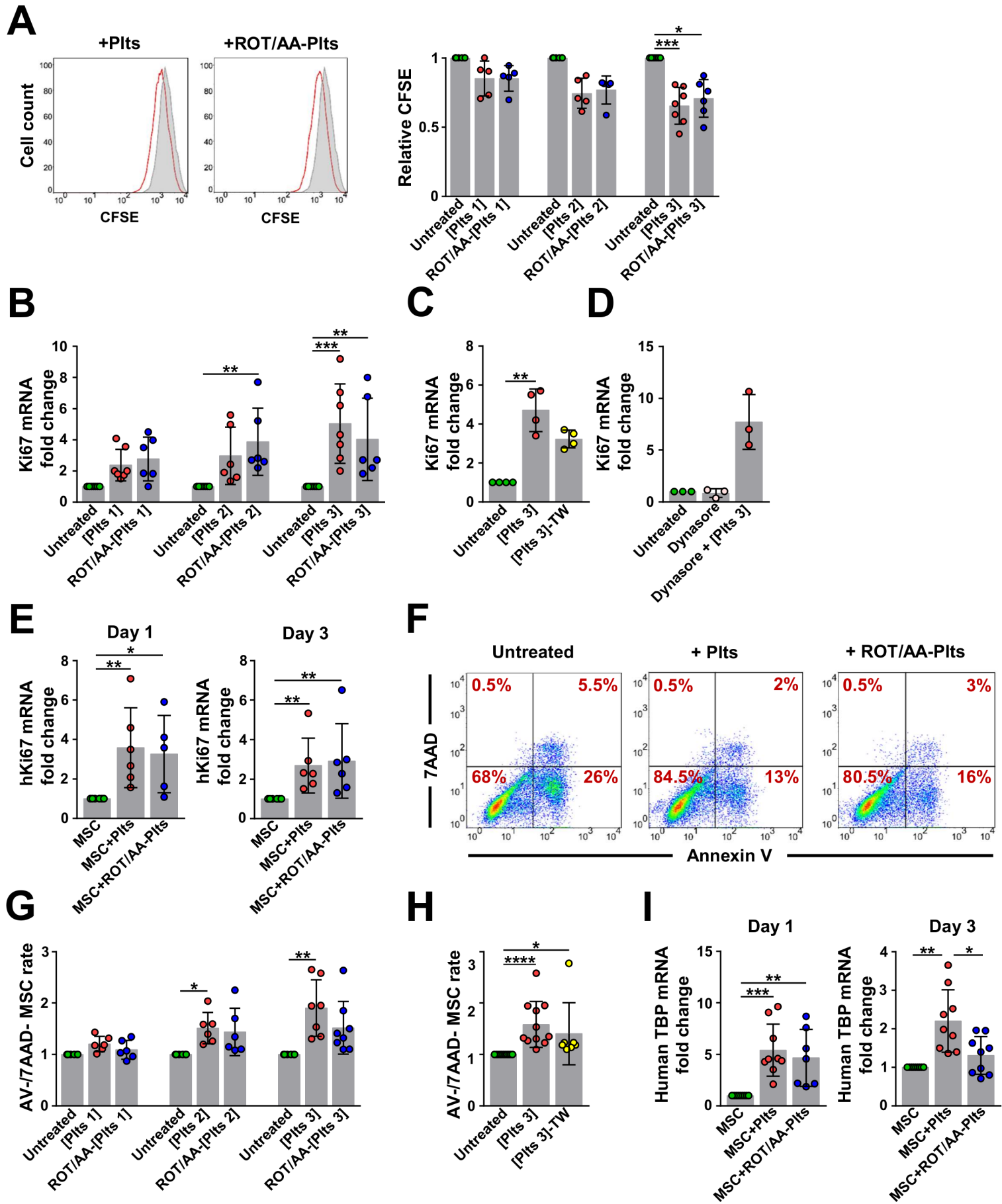
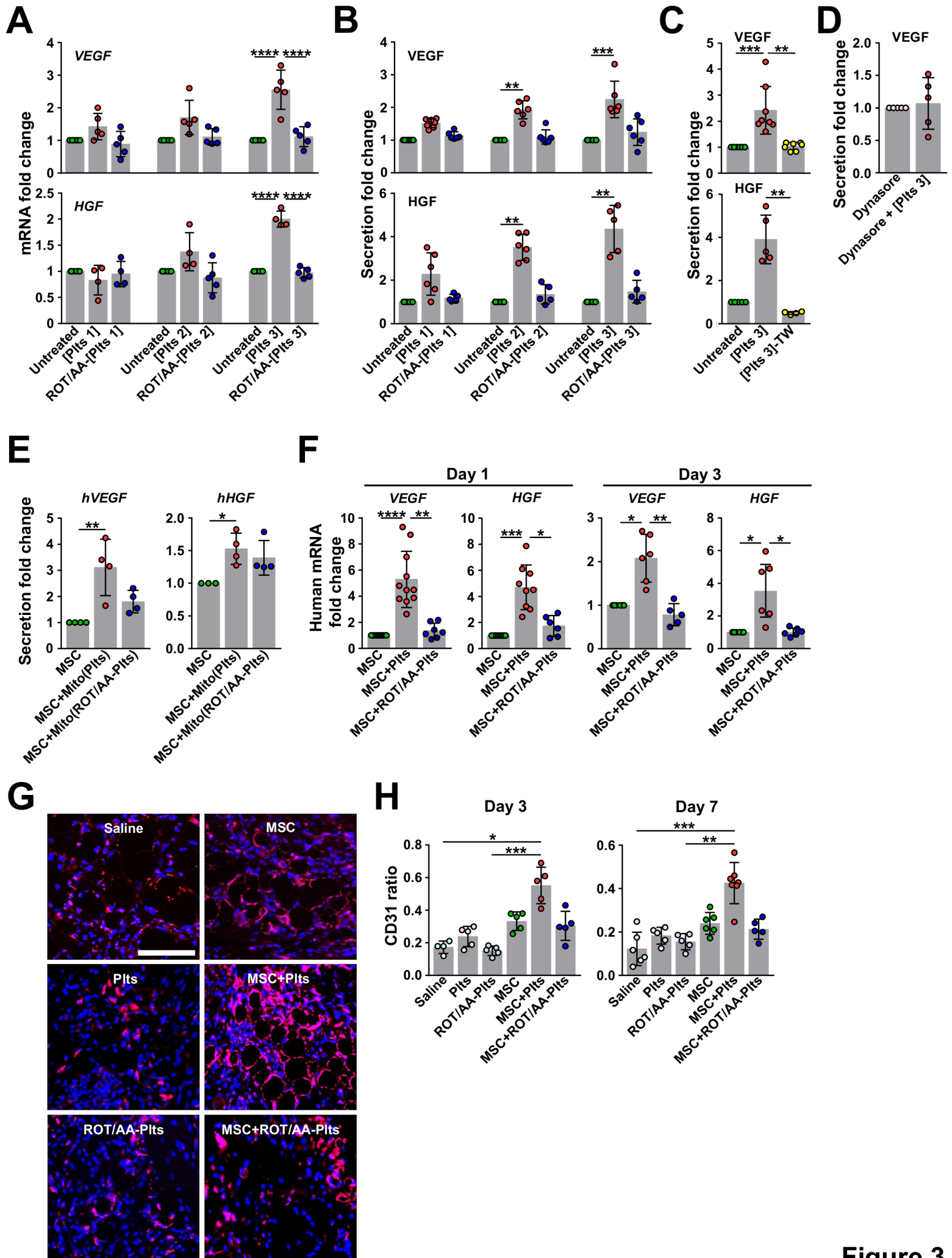


Figure 2



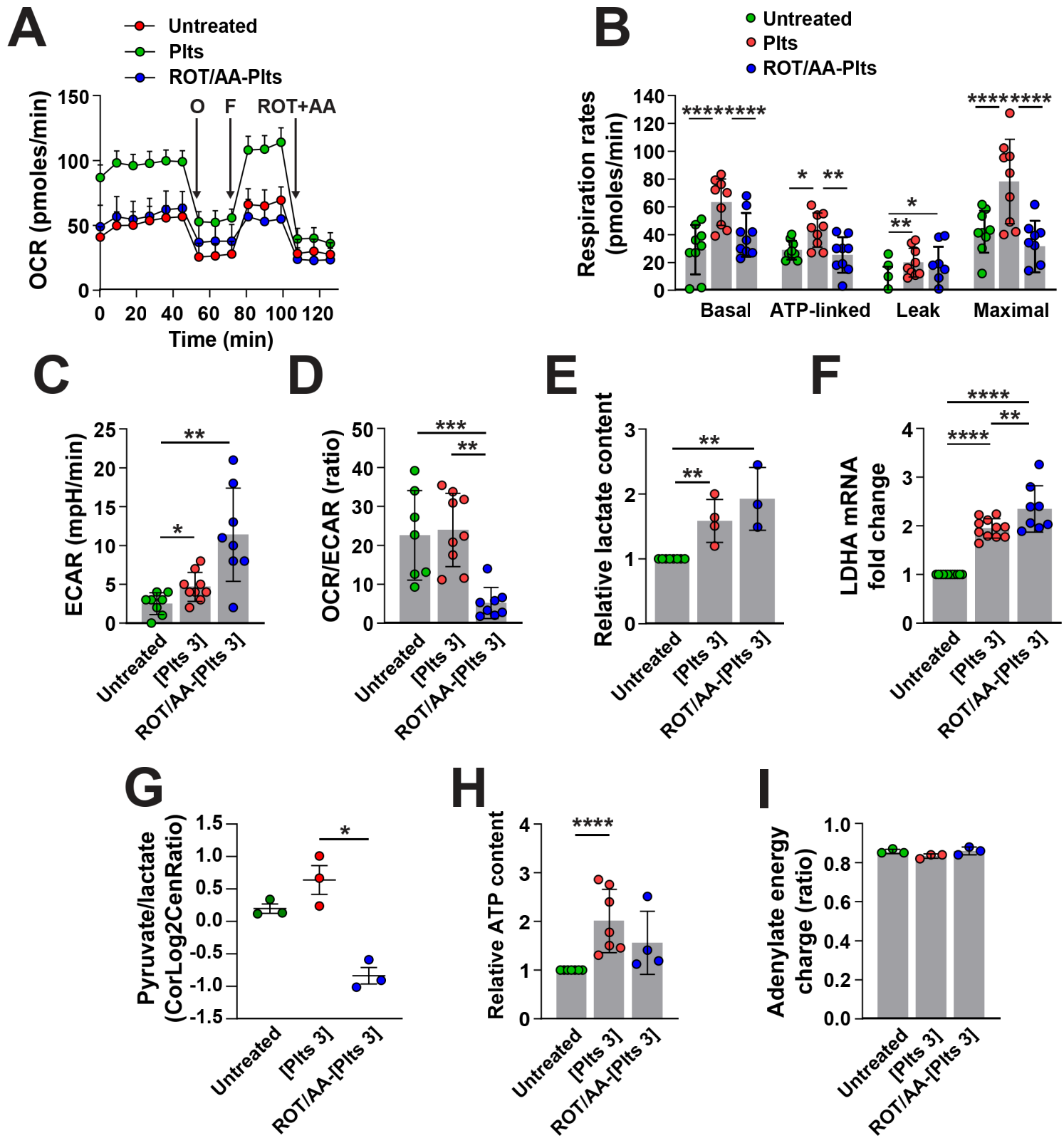


Figure 4

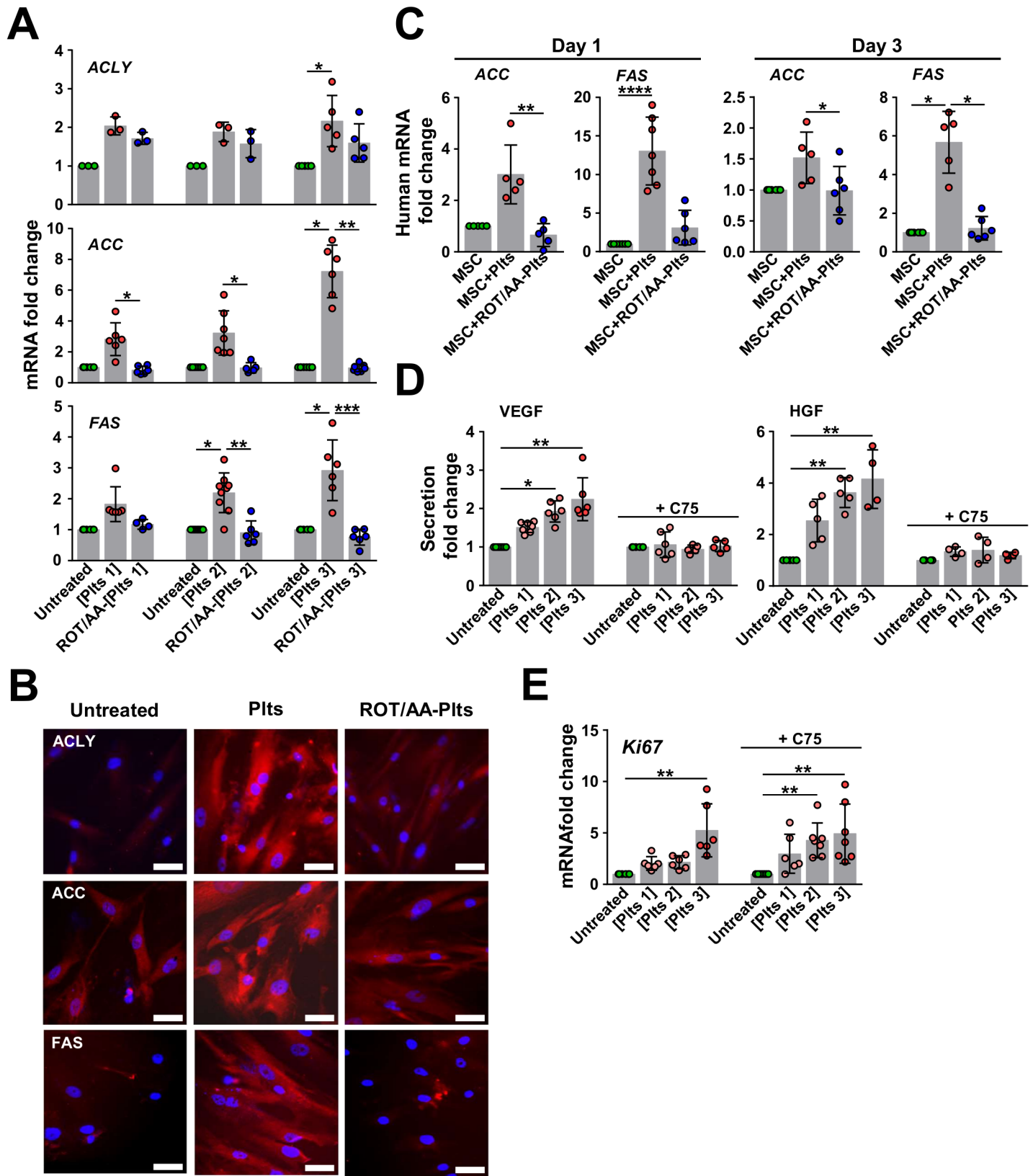


Figure 5

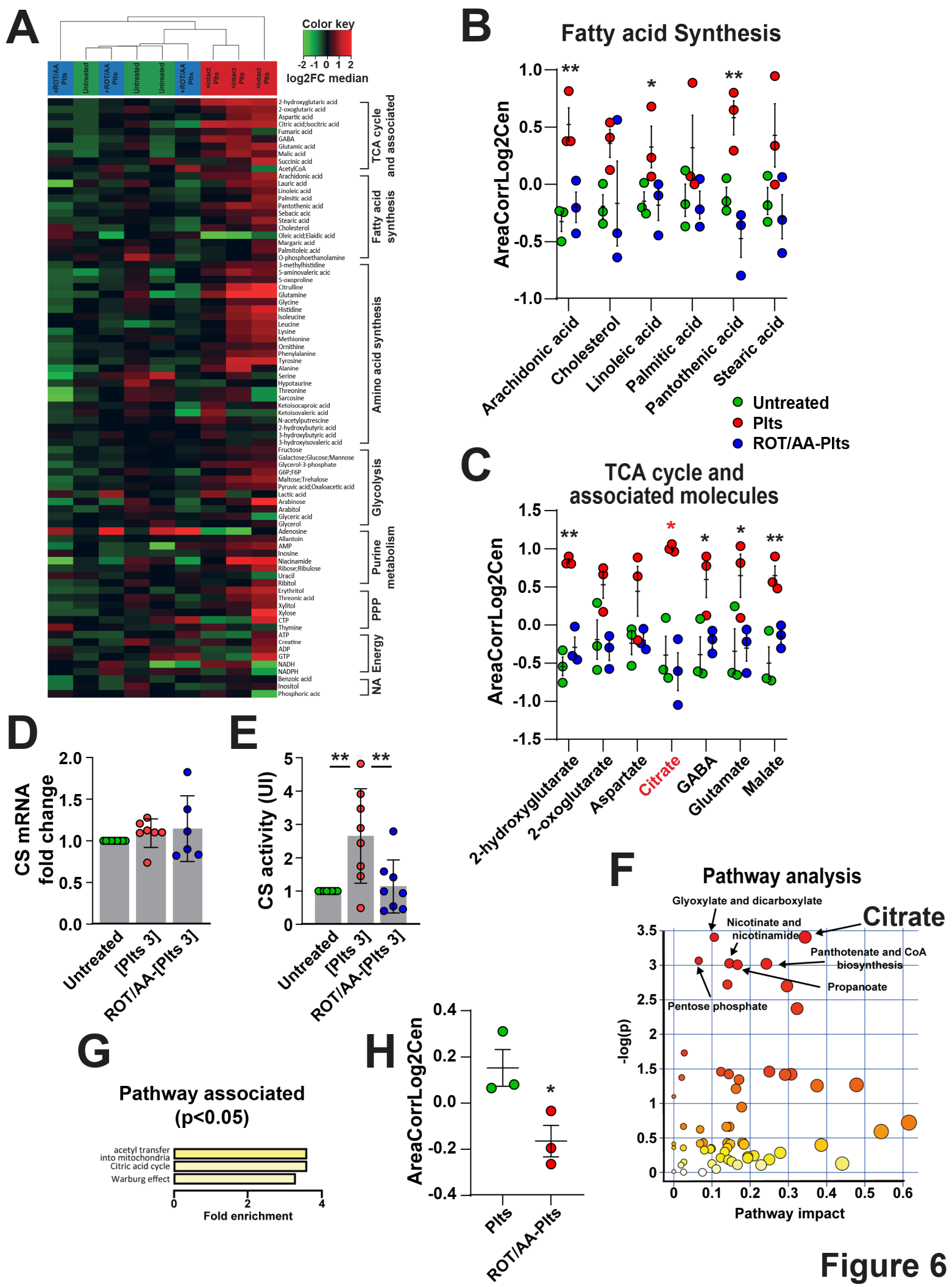


Figure 6

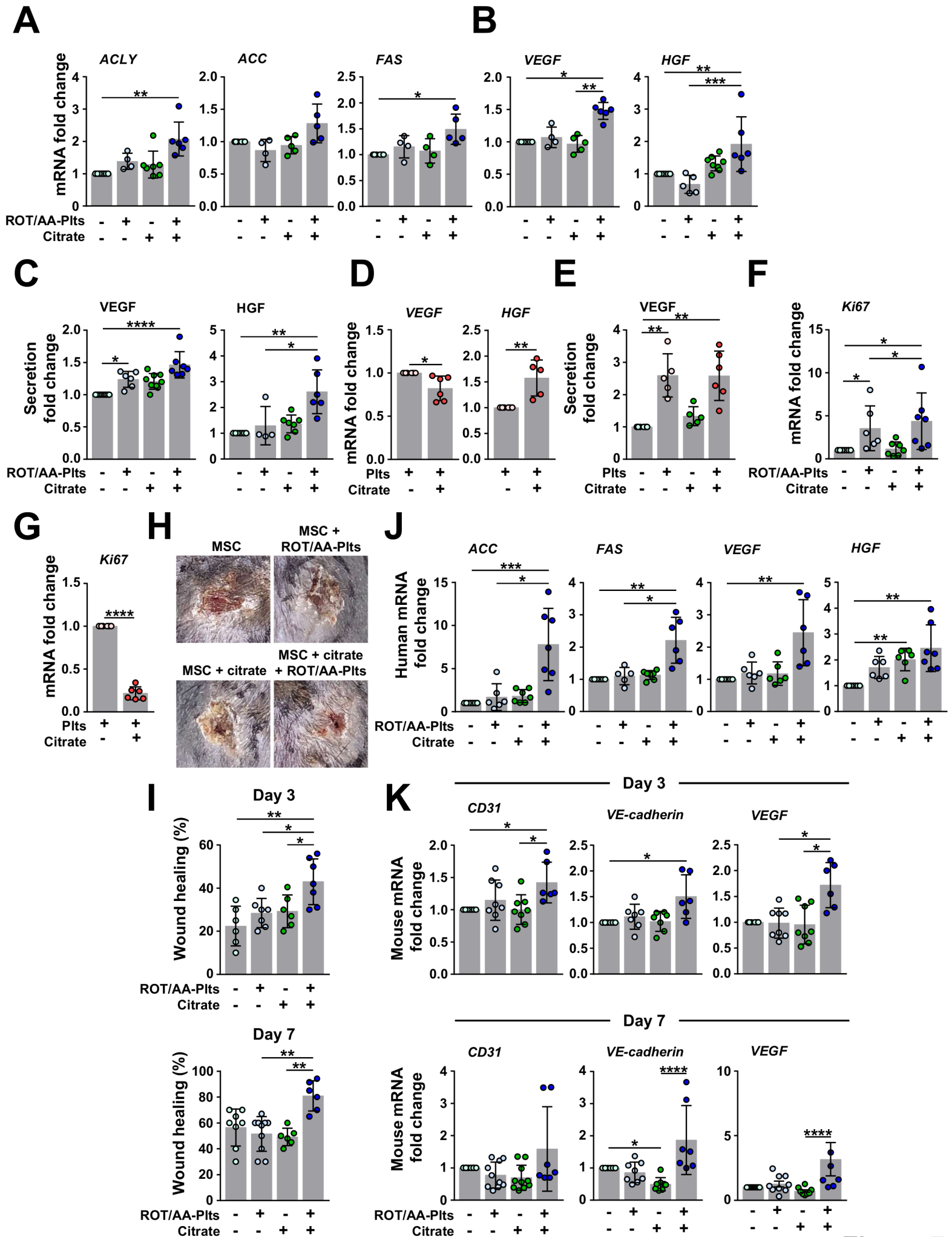


Figure 7

